Novel determinants of NOTCH1 trafficking and signaling in breast epithelial cells

Francis M. Kobia[1,*,+], Luis Castro e Almeida[1], Francesca Carminati[1], Adrian Andronache[2], Francesco Lavezzari[1], Mark Wade[2&] and Thomas Vaccari[1,*]

[1]Dipartimento di Bioscienze, Università degli Studi di Milano, Via Giovanni Celoria, 26, 20133 Milano, Italy

[2]Center for Genomic Science of IIT@SEMM, Fondazione Istituto Italiano di Tecnologia (IIT), Milan, Italy., via Adamello 16, 20139, Milano, Italy

*Corresponding authors: Thomas Vaccari, email: thomas.vaccari@unimi.it, Francis Kobia, email: fkobia@associates.mku.ac.ke

[+]Current address: Mount Kenya University, Department of Research and Innovation, Thika, Kenya

[&]Current address: Astex Pharmaceuticals, Cambridge, UK

Abstract

The evolutionarily conserved Notch pathway controls cell–cell communication during development and in adult metazoans. It influences cell fate decisions, cell proliferation and cell differentiation, and contributes to the maintenance of normal tissue homeostasis. Consequently, misregulation of the Notch pathway is associated with a wide range of diseases, including congenital disorders and cancers with little to no cure. Signaling by Notch receptors is regulated by a complex set of cellular processes that include maturation and trafficking to the plasma membrane, endocytic uptake and sorting, lysosomal and proteasomal degradation, and ligand-dependent and independent proteolytic cleavages. We devised assays to follow quantitively the lifetime of endogenous human NOTCH1 receptor in breast epithelial cells in culture. Based on such analysis, we executed a high-content screen of 2749 human genes for which modulatory compounds exist, to identify new regulators of Notch signaling activation that might be amenable to pharmacologic intervention. We uncovered 39 new NOTCH1 genetic modulators that affect different steps of NOTCH1 cellular dynamics. In particular, we find that *PTPN23* and *HCN2* act as positive NOTCH1 regulators by promoting endocytic trafficking and NOTCH1 maturation in the Golgi apparatus, respectively, while *SGK3* serves as a negative regulator that can be modulated by pharmacologic inhibition. Our findings might be relevant in the search of new strategies to counteract pathologic Notch signaling.

Key words

Notch signaling; intracellular trafficking; Notch trafficking; cell communication

Abbreviations

ADAM: A disintegrin and metalloproteinase; ANK: Ankyrin repeats; APP: amyloid precursor protein; BafA1: Bafilomycin A1; CHX: cycloheximide; CSL: CBF1, Suppressor of Hairless, Lag-1; DAPI: 4',6-diamidino-2-phenylindole; DAPT: N-[(3,5-difluorophenyl)acetyl]-L-alanyl-2-phenyl]glycine-1,1-dimethylethyl ester; DMEM: Dulbecco's modified eagle medium; DMSO:

dimethyl sulfoxide; DSL: Delta/Serrate/Lag2; EDTA: ethylenediaminetetraacetic acid; EGTA: ethylene glycol tetraacetic acid; EGF: epidermal growth factor; EGFR: epidermal growth factor receptor; ESCRT: endosomal sorting complexes required for transport; esiRNA: endoribonuclease-prepared siRNAs; ER: endoplasmic reticulum; GA: Golgi apparatus; GSI: gamma (γ)-secretase inhibitor; HCS: high content screen; HCN2: hyperpolarization-activated cyclic nucleotide-gated channel 2; HES1: hes family bHLH transcription factor 1; HEY1: hes related family bHLH transcription factor with YRPW motif 1; HRP: horse radish peroxidase; IF: immunofluorescence; KD: knockdown; MGV: mean gray value; N1FL: NOTCH1 full length; N1ICD: NOTCH1 intracellular domain; ns: not significant; NT: Non-targeting; N1TM: NOTCH1 transmembrane; OTP: ON TARGET plus; PFA: paraformaldehyde; PM: plasma membrane; pNDRG1: phospho-N-myc downstream regulated gene 1; PSENEN: presenilin enhancer gamma secretase subunit; PTPN23: protein tyrosine phosphatase non-receptor type 23; RTN3: reticulon 3; S1: Notch cleavage site 1; S2: Notch cleavage site 2; S3: Notch cleavage site 3; SGK3: serum/glucocorticoid regulated kinase family member 3; siRNA: short interfering RNA; Su(Dx): supressor of deltex; TGN46: TGOLN2 (trans-golgi network protein 2); V-ATPase: vacuolar H^+ ATPase; w/o: washout; λ-PPA: lambda phosphatase.

Introduction

The evolutionarily conserved Notch pathway is a form of direct cell–cell communication that is extensively deployed in the regulation of multiple cellular functions during development and in adults. It influences cell fate decisions, cell proliferation and cell differentiation, and contributes to the maintenance of normal tissue homeostasis in both invertebrate and vertebrate metazoans [1–3]. As a consequence of such broad function, loss or gain of Notch function is associated with several congenital disorders [4] and cancers (Aster et al., 2017).

Upon synthesis in the endoplasmic reticulum (ER), Notch proteins are processed at site S1 by Furin in the TGN (Trans Golgi Network), the distal portion of Golgi apparatus (GA). Such

cleavage generates the mature receptors exposed on the cell surface that are held together by Ca^{2+} coordination within the heterodimerization domain (HD; see Fig. 1A for a schematic of human NOTCH1) [5,6]. Once at the cell surface, Notch receptor activation can be initiated by binding the Delta/Serrate/Lag2 (DSL) family of Notch ligands that are present on the surfaces of adjacent signal-sending cells [7]. Following ligand binding, the receptors undergo two activating proteolytic cleavages; the first one is extracellular and is executed by ADAM10 at site S2 [8]. The second is intracellular and is mediated at site S3 by the γ-secretase complex [9–11] (see Fig. 1A for a schematic of human NOTCH1). These cleavages generate the transcriptionally competent NICD (Notch Intracellular Domain) which translocates to the nucleus and activates the expression of Notch target genes [12]. In addition, Notch signaling activation may occur through non-canonical means on the endosomal surface, with or without stimulation by ligands [13,14].

As a membrane-tethered transcription factor, the Notch signaling output is not only controlled by ligands, ADAM metalloproteases, the γ-secretase complex and the CSL transcriptional complex, but also through intracellular trafficking [2,12,15–18]. Indeed, loss or modulation of various activities occurring at membranes positively or negatively impact signaling in both model organisms and humans. These activities include glycosylation enzymes [19–21], internalization regulators such as Dynamin [22], and ubiquitin ligases such as Dx (Deltex) [23–27], Su(Dx) (suppressor of Deltex)/AIP4/ITCH in mammals [28,29], and NEDD4 [17,30]. In addition, components of the endo-lysosomal system, such as Endosomal Sorting Required for Transport (ESCRT) proteins [31–33] or the vacuolar-ATPase (V-ATPase) pump are required for endocytic Notch trafficking and signaling [34–40]. It is plausible that numerous other factors, yet to be identified and characterized, contribute to fine tune Notch liberation from membranes signaling by harnessing the intracellular trafficking machinery. Thus, aiming to improve knowledge of Notch receptor trafficking and to identify novel genes that control Notch trafficking and signaling, here we combine quantitative immunofluorescence, RNA interference, and automated microscopic imaging to describe the kinetics of endogenous NOTCH1 export to the plasma

membrane (PM), and its endocytic uptake and lysosomal clearance in human epithelial mammary gland cells in culture. Finally, we screen to identify novel modulators of Notch trafficking and signaling.

Materials and methods

Cell culture

MCF10A cells (ATCC, Cat #: CRL-10317) were cultured in DMEM/F12 (ThermoFisher Scientific, Cat #: 11320033) supplemented with 5% Horse Serum (ThermoFisher Scientific, Cat #: 16050122), 10 mg/ml insulin (Merck Life Sciences, Cat #: 11376497001), 0.5 mg/ml Hydrocortisone (Merck Life Sciences, Cat #: H0888-5G), 100 ng/ml cholera toxin (Merck Life Sciences, Cat #: C8052-2MG) and freshly added 20 ng/ml EGF (Vinci-Biochem, Cat #: 90201-3). The MCF10A-RbpJk-Luc Notch signaling reporter cell line, which carries a luciferase gene under the control of a Notch promoter, was maintained under antibiotic selection in normal MCF10A medium supplemented with puromycin (Vinci-Biochem, Cat #: AG-CN2-0078-M100) at a final concentration of 2 mg/ml.

Compounds and chemicals

Where indicated, cells were treated with the following compounds and/or chemicals at indicated concentrations. γ-secretase inhibitor: DAPT (Santa Cruz Biotechnology, Cat #: sc-201315), V-ATPase inhibitor: BafA1 (Santa Cruz Biotechnology, Cat #: sc-201550), SGK3 inhibitor: VPS34-IN1 (Selleckchem, Cat #: S7980). Stock solutions of the compounds were prepared in cell culture grade DMSO (EuroClone, Cat #: EMR385250). λ-phosphatase (λ-PPA) along with 10X λ-PPA reaction buffer and 10X $MnCl_2$) was purchased from Santa Cruz Biotechnology (Cat #: sc-200312A). EGTA was purchased from Santa Cruz Biotechnology (Cat #: sc-3593D).

EGTA stimulation of Notch cleavage, nuclear translocation and signaling

Notch signaling activation was stimulated by Ca^{2+} depletion [6]. For short-term Ca^{2+} removal, EGTA was added at a final concentration of 10mM for up to 30 minutes, while for extended periods, EGTA was used at a final concentration of 2.5mM for 2–4 hours, followed by downstream assays.

Immunofluorescence

Immunofluorescence (IF) was performed on cells grown on coverslips. For IF staining, cells were fixed for 10 minutes with 4% PFA at room temperature. They were then rinsed thrice with PBS 1X and then permeabilized for 10 minutes with 0.1% triton-PBS 1X or with 0.01% saponin in PBS. They were then incubated in 3% BSA in PBS 1X blocking solution or in 0.01% saponin in PBS for 30 minutes and then incubated with primary antibody dissolved in the appropriate blocking solution for 1 hour at room temperature. Excess antibody was washed off by rinsing 3 times with PBS 1X, 5 minutes each. Samples were then incubated in secondary antibody diluted in the appropriate blocking solution for 1 hour at room temperature followed by three washes using PBS 1X, 5 minutes per wash. The following primary antibodies were used: rat anti-full length NOTCH1, 5B5 monoclonal antibody (Merck Life Sciences, Cat #: SAB4200024) at 1:300, Goat anti-EEA1 (Santa Cruz, Cat #: sc-6415) at 1:150, Rabbit anti-GIANTIN (Covance, Cat #: PRB-114C) at 1:1000, Rabbit anti-TGN46 (Proteintech, Cat #:13573-1-AP) at 1:300, and Rabbit anti-LAMP1 (Merck Life Sciences, Cat #: L1418) at 1:200 (requires permeabilization with saponin). Cell surface membranes were marked with phalloidin (Merck Life Sciences, Cat #: P5282) at 1:100 and the nuclei counterstained with DAPI (Merck Life Sciences, Cat #: D9542) at 1:1000. Confocal image acquisition was done using a Leica TCS SL confocal system. Where noted, digital images were processed using Photoshop or ImageJ software without biased manipulation.

ImageJ was used for quantitative analysis of IF images. To assess colocalization in co-stained samples, imaging channels were first separated using the split channel function of ImageJ. To quantify NOTCH1 accumulation in the Golgi in *HCN2*-silenced conditions, ImageJ's freehand selection tool was used to trace a region of interest (ROI) on the GIANTIN, Golgin-97, or TGN46 channel. The marked ROIs were then transferred onto the NOTCH1 channel using the ROI manager tool. Next, the mean gray value (MGV) was measured to determine the size of the Golgi and the level of NOTCH1 intensity. For NOTCH1 quantification at the plasma membrane (PM), a ROI was traced on the inside (cytosolic side of the PM) and on the outside (external side of the PM) based on NOTCH1 signal on the cell membrane and the MGV measured. To get the proportion of NOTCH1 in either compartment, the MGV of each ROI (in the NOTCH1 channel) was divided by the cell's total MGV on the NOTCH1 channel. A total of eight *HCN2* KD and eight control images, 5 ROI per image, were quantified. To quantify the number of endo-lysosomal puncta, NOTCH1-positive puncta, and the rate of NOTCH1 colocalization with the markers EEA1 (early endosomes), LAMP1 (late endosomes/lysosomes), and Golgin-97 (GA) in *PTPN23*- or *SGK3*-silenced samples, ImageJ's freehand selection tool was used to trace the cytoplasmic area between the edge of the nucleus and the inner side of the PM on the merged (NOTCH1+DAPI+EEA1 or NOTCH1+DAPI+LAMP1) composite image. The ROI manager was then used to transfer the identified ROI onto individual channels and the number of NOTCH1-, EEA1-, Golgin-97-, or LAMP1-positive puncta identified and counted using ImageJ's ComDet v.0.5.5 plugin (DOI: https://doi.org/10.5281/zenodo.6546038) after empirically determining the spot detection thresholds on each channel. For spot (puncta) identification, the intensity threshold was set at 4 and colocalization determined using a maximum distance of 2 pixels between colocalized puncta as threshold. To determine the rate of puncta colocalization, the NOTCH1 channel was merged with the EEA1, LAMP1, or Golgin-97 channel to generate a composite image on ImageJ and the ComDet plugin used to measure particle colocalization. At least 5 ROIs, in at least five images were analyzed.

Western blot analyses

For western blot analyses, cells were scraped into 1 ml of the media they had been cultured in, transferred into prechilled 1.5 ml Eppendorf tubes, and placed on ice. They were then centrifuged at full speed (14,000 rpm) for 5 minutes at 4°C and the pellets rinsed once with ice-cold PBS 1X. Unless indicated otherwise, cell pellets were then lysed by resuspension in 60 µl ice-cold RIPA buffer (ThermoFisher Scientific, Cat. #: 89901) supplemented with a protease inhibitor cocktail (Merck Life Sciences, Cat #: 11697498001). They were then vortexed for 10 seconds, incubated on ice for 15 minutes, cleared by centrifugation at full speed for 20 minutes at 4°C, and the supernatants transferred into fresh 1.5 ml Eppendorf tubes on ice. Protein concentrations were quantified using a BCA protein assay kit (ThermoFisher Scientific, Cat #: 233225) following manufacturer guidelines. Next, for each sample, 20 µg of the protein lysate were mixed with 7.5 µl of 4X Laemmli sample buffer (Bio-Rad Laboratories, Cat #: 1610747) containing 10% β-mercaptoethanol (Bio-Rad, Cat #: 1610710) and the volume topped up to 30 µl using distilled water. Depending on target protein molecular weight, the samples were then resolved on precast 4–20% Criterion™ TGX Stain-Free™ polyacrylamide gels (Bio-Rad, Cat #: 5678094) or 7.5% stain-free gels (Bio-Rad, Cat #: 4568024 or 5678024) polyacrylamide gels using 1X Tris/Glycine SDS running buffer (Bio-Rad, Cat #: 1610732). Proteins were then transferred onto 0.2 µm nitrocellulose membranes using Trans-Blot® Turbo™ Mini Nitrocellulose Transfer Packs (Bio-Rad, Cat #: 1704158EDU) on a Trans-Blot Turbo TM Transfer System (Bio-Rad, Cat #: 1704150). Protein transfer was then visualized using 0.1 % Ponceau S solution (w/v) in 5% acetic acid (Merck Life Sciences, Cat #: P7170-1L) and imaged. The membranes were then washed using 1X TBS (Bio-Rad, Cat #: 1706435) containing 0.1% Tween-20 (Bio-Rad, Cat #: 1610781) – TBST, for 15 minutes and then blocked with 5% skimmed milk (Merck Millipore, Cat #: 70166) in TBST for 3 hours. Membranes were then incubated overnight at 4°C in the following primary antibodies: rabbit anti-cleaved Notch1 (Val 1744) at 1:1000 (Cell signaling technology, Cat #: 4147S), rabbit anti-Notch1 (D1E11) XP® at 1:1000 (Cell signaling technology, Cat #:

3608S), mouse anti-Vinculin at 1:5000 (Bio-Rad, Cat #: MCA4665GA), mouse anti-β-actin at 1:5000 (Merck Life Science, Cat #: A-5441), or rabbit anti-Phospho-NDRG1 (Thr346) (D98G11) XP® at 1:1000 (Cell signaling technology, Cat #: 5482). Membranes were then washed thrice with TBST (5 minutes/wash) at room temperature and then incubated with HRP-conjugated goat anti-rabbit IgG (H + L) (Bio-Rad, Cat #: 170-6515) or goat anti-mouse IgG (H + L) (Bio-Rad, Cat #: 170-6516), both at 1:5000, for one hour at room temperature. They were then washed thrice with TBST (5 minutes/wash) at room temperature and signal developed for one minute using Clarity™ Western ECL substrate (Bio-Rad, Cat #: 1705060) or Clarity Max Western ECL Substrate (Bio-Rad, Cat #: 1705062). They were then imaged on a ChemiDoc MP imaging system (Bio-Rad). Band intensities were quantified using Image Lab software (Bio-Rad) followed by statistical analysis and graph visualization using GraphPad Prism.

Lambda phosphatase (λ-PPA) treatment

For the λ-PPA assay, two types of RIPA lysis buffer were used – RIPA supplemented with protease (phenylmethylsulfonyl fluoride and 1 tablet of 1X cOmplete mini protease inhibitor cocktail, EDTA-free) and phosphatase (sodium fluoride and sulfur monoxide) inhibitors, and RIPA supplemented with protease inhibitors only (phenylmethylsulfonyl fluoride and 1 tablet of 1X cOmplete mini protease inhibitor cocktail, EDTA-free). The first lysis buffer (containing phosphatase inhibitors) was used as a negative control for phosphatase treatment. MCF10A cells were harvested, lysed in the appropriate ice-cold RIPA buffer (with or without phosphatase inhibitor), and protein quantified as described in section 2.5. Next, for each sample (protein concentration: 1 µg/µl), 25 µg of protein (25 µl) were subjected to λ-PPA treatment following manufacturer instructions. Briefly, 0.5 µl of λ-PPA (20,000 U) were added into each tube (containing 25 µl of the sample), along with 3.2 µl of 10X λ-PPA buffer and 3.2 µl of 10X $MnCl_2$ (final volume: 32 µl). The samples were then mixed by gently flicking the tube and incubated for 30 minutes at 30°C. Next, 10.75 µl of 4X Laemmli loading buffer were added into each sample,

followed by western blotting using the antibody against the γ-secretase-cleaved (Val1744) NOTCH1 intracellular domain (N1ICD).

Cycloheximide treatment and assessment of NOTCH1 protein stability

Where indicated, after gene knockdown for 72 hours, MCF10A cells were treated with 10 μM cycloheximide (CHX) to block protein synthesis or an equal volume of DMSO (vehicle) for 4 hours. Cells were then harvested, lysed, and protein concentration quantified as described in section 2.5. To assess NOTCH1 protein stability, 20μg of the protein lysate per sample were subjected to western blot analysis using the antibody against full length NOTCH1 (N1FL) and transmembrane NOTCH1 (N1TM), as well as the antibody against the γ-secretase-cleaved N1ICD. Band intensities were then analyzed on GraphPad Prism to determine the differences between the levels of N1FL, N1TM, and N1ICD in the CHX-treated vs untreated cells.

Gene silencing

Gene knockdowns were performed in 384-well plate format. Each gene/well was targeted with a pool of four distinct siRNAs against different sequences of the respective target transcript. Each of the 10 libraries was knocked down in 6 replicates. Three of the replicates were subjected to EGTA stimulation while the other 3 were left unstimulated. For siRNA transfection, cells were always maintained at less than 6 passages and trypsinized for transfection while at 60%–80% confluence. All siRNA transfections were done in black 384-well, tissue culture treated optical plates (Corning, Cat #: 3712), using the reverse transfection method. Briefly, desired siRNAs were diluted in Optimem (ThermoFisher Scientific, Cat #: 51985-042) at a concentration of 50 nM, complexed with 0.12 μl of Lipofectamine™ RNAiMAX Transfection Reagent (ThermoFisher Scientific, Cat #: 13778500) per 20 μl of Optimem-siRNA solution for 20 minutes at room temperature, and 20 μl of the complex dispensed into each 384 well. Where indicated, esiRNA was used at a final concentration of 50 nM. Cells were suspended at a density of 35 cells/μl in 2X MCF10A cell culture media and 20 μl of the cell suspension (700 cells) added into each well

(containing 20 µl of the transfection complex) to obtain a final siRNA concentration of 25 nM. The 2X medium was prepared using each component of the medium at double its standard concentration. Double the concentration of EGF shown in section 2.1 was added fresh into the cells before they were added into the wells. Cells were then cultured for 72 hours as described in section 2.1, in a SteriStore™ automated incubator (HighRes Biosolutions). All solutions were dispensed using the Freedom EVO automated liquid handler system (Tecan).

To stimulate NOTCH1 activation, at the end of the 72 hours of gene knockdown, 3 plates from each library were treated with EGTA for 2 hours to stimulate Notch cleavage. To do this, 10 µl of fresh media containing 12.5 mM EGTA was directly added into the wells to a final concentration of 2.5 mM EGTA per well, and a final volume of 50 µl/well. The NoEGTA stimulation plates received 10 µl of sterile water. The plates were then incubated for 2 hours at 37°C and then fixed with 2% PFA for 15 minutes at room temperature. Fixation was done by adding 50 µl of 4% PFA directly into the wells. Solutions were dispensed into the wells using a Multidrop™ Combi Reagent Dispenser (ThermoFisher Scientific).

Automated immunofluorescence analyses

Automated immunostaining for high content screening (HCS) was performed using a Biotek EL406 washer/dispenser equipped with a 192-tube aspiration manifold. The solution was removed from the wells and the cells rinsed once with 1X PBS. Cells were permeabilized with 0.05% triton in 1% BSA blocking solution for 1 hour at room temperature followed by a single wash with 1X PBS. Cells were then incubated for 1 hour at room temperature with the anti-NOTCH1 primary antibody (Merck Life Sciences, Cat #: SAB4200024) diluted at 1:350 in 1% BSA blocking solution. The primary antibody solution was then removed, and the plates washed twice with 1X PBS. Next, the cells were incubated for 1 hour with 1% BSA blocking solution containing DAPI at 1:4,500 (Merck Life Sciences, Cat #: D9542), phalloidin at 1:350 (Merck Life Sciences, Cat #: P5282), and Alexa Fluor 488 anti-rat secondary antibody at 1:400 (ThermoFisher Scientific,

Cat #: A21208). They were then washed thrice with 1X PBS before imaging. Where imaging could not be performed immediately, the immunostained cells were stored at 4°C for not more than 48 hours prior to image acquisition.

Automated image acquisition

The 384-well plates were scanned using an automated Olympus Scan^R (Tokyo, Japan) microscope equipped with a Hamilton arm for plate handling. Eight fields of view and three emission fluorescent channels (DAPI, phalloidin, and Alexa 488), were acquired for each well using a 20X objective. Imaging data were annotated and transferred to the Isilon infrastructure and network software and indexed by plate barcode for storage. In the annotation each well was assigned information regarding the date of the experiment, the gene knocked down, the sub-genomic library the knocked down gene belongs to, and the treatment (EGTA vs NoEGTA). Images were then uploaded to the Columbus server (PerkinElmer), where they could be accessed for visual examination and automated analysis.

High content screen image analysis

An in-house Acapella (PerkinElmer) image analysis script was developed and used for batch image analysis and to quantitatively describe a set of phenotypic features. All analyzed images were first subjected to background correction and exclusion of unevenly illuminated images. Background correction was done separately for each channel. DAPI, which was used to mask the nuclei and phalloidin, which labeled cell surfaces, were used for cell segmentation. Segmentation was performed using a modified version of the watershed algorithm, which allowed the inversion of phalloidin channel images so as to display high pixel intensities in the cell and low intensities along the cell membrane, allowing application of the watershed approach to identify cell boundaries. This algorithm also detects and excludes regions of the image fields not covered by cells. Once the cells, their membranes, and corresponding nuclei were detected, each cell was segmented into the nucleus based on DAPI staining, the membrane based on phalloidin signal,

and the cytosol (region between the nuclei and cell surface membrane). Cells that were adjacent to field of view borders, those deemed to be too small or too big, those with saturated pixel intensities or those that were improperly segmented, were excluded from downstream image analysis. To exclude out-of-focus images, we used boxplot statistics on the distribution of intensity contrast values (on the DAPI channel) of all nuclei detected in the entire well. Using the first and the third quantiles of this distribution, we estimated the lower inferior fence (LIF) using the 95% confidence interval. For each field of view, we next established the number of nuclei presenting a contrast lower than the LIF and classified fields in which >50% of the nuclei failed to cross the LIF threshold as being out of focus. Data analysis on the EGTA stimulated plates was performed independently of the corresponding non EGTA-treated plates. For each gene (well), the parameters of interest were quantified and reported as z-score values [41].

Candidate gene selection for validation

For each library plate, candidate genes from the EGTA and the NoEGTA conditions were considered to affect respective parameters if their knockdown shifted the z-score positively or negatively, the further the shift, the stronger the phenotype. The main parameters quantified were, a) cell viability (QC1_NoOfAnalysedCells), b) Overall Notch intensity in the cell (N4_CellNotch), c) nuclear Notch intensity (N1_NucNotch), d) cell surface membrane Notch intensity (N3_MembNotch), and e) Notch accumulation in intracellular compartments (N5_PercentOfCellsWithSpots & N9_NoOfSpotsPerCell).

Generation of the stable Notch signaling reporter cell line, MCF10A-RbpJk-Luc

A Notch pathway transcriptional output reporter cell line was generated by infecting MCF10A cells with Cignal Lenti RBP-Jk Reporter (luc) lentiviral particles (Qiagen, Cat #: CLS-014L) following manufacturer instructions. This reporter system carries an inducible RBP-Jk-responsive firefly luciferase reporter as well as a puromycin resistance gene that permits the selection of cells that stably integrate the reporter construct. To isolate stably infected single cell

clones, the cells were counted and serially diluted in order to have a final concentration of 2.5 cells/ml. Next, 200µl of the cell suspension were seeded onto four 96-well plates so as to have 0.5 cells/well. The cell culture medium was changed twice a week and in the second week the cells were examined for single cell clones. Each of the healthiest looking clones, but with a slightly different cell morphology relative to normal MCF10A cells were selected, transferred onto 48-well plates, grown while observing the growth characteristics, and then transferred into 6-well plates after reaching 70%–80% confluence. Eventually each single cell clone population was split into two wells of a 6-well plate and frozen after reaching 70%–80% confluence, followed by long term storage in liquid nitrogen. Each clone was then tested using a luciferase assay for Notch signaling inducibility using EGTA. The two best clones with the widest Notch signaling induction assay window, measured as the ratio between basal luciferase activity (in the absence of EGTA) to activated luciferase activity (in the presence of EGTA), clone 1 and clone 13, were selected for further characterization.

To assess the ability to activate and control the Notch pathway in the stable Notch reporter cell lines, MCF10A-RbpJk-Luc single cell clones were seeded on white, opaque, flat-bottomed 96 well plates (Merck Life Sciences, Cat #: CLS3362-100EA) at 9,000 cells, in 100 µl of medium and grown overnight. Notch signaling was then stimulated by adding 11 µl of media supplemented with 25 mM EGTA into each well to reach a final concentration of 2.5 mM EGTA in 111 µl of medium. The cells were then incubated with EGTA for 2 hours to allow Notch signaling activation and resulting luciferase synthesis. The luciferase assay was then performed by adding 9 µl of fresh medium containing 6.6 mM of D-luciferin into each well to have a final concentration of 500 µM D-luciferin per well, in a final volume of 120 µl per well. The cells were then incubated for 2 hours after which luminescence readings were taken on a Promega Glomax multimode plate reader. To assess the ability to block Notch signaling activation in the reporter cell line, we silenced *NOTCH1*, *PSENEN,* and *ADAM10* for 72 hours using siRNA (Dharmacon) before Notch signaling activation and the luciferase assay. To account for reductions in cell proliferation upon

gene silencing, a cell viability assay was performed after the luciferase assay by adding 12 µL of resazurin (Merck Life Sciences, Cat #: TOX8-1KT) and the cells incubated for an additional 2 hours followed by fluorescence reading on a Promega Glomax multimode plate reader.

Secondary screen for signaling activity

Relevant genes were knocked down in MCF10A-RbpJK-Luc Notch signaling reporter cells, on white opaque 384-well plates (Corning, Cat #: 3712) followed by luciferase/proliferation assays using 500 µM D-luciferin and 2.5% resazurin after 72 hours. Where indicated EGTA was used at a final concentration of 2.5 mM. Briefly, a mix of D-luciferin+resazurin was prepared immediately before the experiment by dissolving D-luciferin and resazurin in normal MCF10A cells media at a concentration 3.6X higher than the desired final concentration. Where EGTA-stimulated Notch activation was desired, a mix of D-luciferin+resazurin+EGTA was prepared by including EGTA at a concentration 3.6X higher than its desired final concentration. Next, 15 µl of the appropriate solution of Notch luciferase assay mix was added into each well of the 384-well plate and the cells incubated for 4 hours in normal conditions. To assess Notch signaling output (luminescence) and cell viability (resazurin fluorescence), luminescence and fluorescence were read on a PHERAstar BMG LABTECH microplate reader.

Statistical analyses

All experimental data were analyzed on GraphPad Prism. All data represent at least 3 independent replicates and are shown in graphs as individual values, mean ± SD, or normalized values. Statistical differences between two groups were evaluated using unpaired two-tailed Student's t-tests, with *, **, ***, ****, and ns indicating $p < 0.05$, $p < 0.01$, $p < 0.001$, $p < 0.0001$, and not significant, respectively. Data and statistical analyses for the screen were done as described in section 2.11.

Acknowledgements and funding information

We thank Fernanda Ricci and Michela Mattioli for excellent technical help during the execution of the HCS. This work is supported by AIRC (Associazione Italiana Ricerca sul Cancro) IG grant 20661 to TV and by IIT@SEMM.

Author contributions

FMK and TV designed the study. FMK, LCA, FC and FL conducted the experiments. AA performed the computational analyses of the screening data. MW coordinated the execution of the HCS screen. TV wrote the manuscript with the help of FMK and LCA.

Results

Canonical NOTCH1 signaling in human MCF10A cells

Knowledge about Notch signaling dynamics is a prerequisite to investigating factors that control signaling by modulating its trafficking to subcellular compartments. MCF10A cells, derived from non-transformed human breast epithelial cells [42], express Notch signaling pathway ligands and receptors including *NOTCH1*, *NOTCH2*, and *NOTCH3*, while *NOTCH4* is not detectable [34]. Immuno-localization with an antibody that recognizes the intracellular domain of NOTCH1, shows that endogenous NOTCH1 is localized on the cell surface in MCF10A cells (Fig. 1B). As expected, efficient knockdown (KD) of key components of the Notch signaling pathway, such as *ADAM10* (encoding the S2 cleavage metalloprotease) and *PSENEN* (encoding a γ-secretase component necessary for S3 cleavage) in MCF10A cells prevented the translocation of endogenous NOTCH1 into the nucleus upon EGTA-mediated Ca^{2+} chelation (Fig. 1B–C; materials and methods). Consistent with this, *NOTCH1*, *ADAM10* or *PSENEN* depletion significantly suppressed EGTA-stimulated Notch signaling, when measured in MCF10A cells stably expressing the Notch activation reporter RBPj-luc (Fig. 1D).

We previously observed that the S3-cleaved NOTCH1 intracellular domain (N1ICD) is visible in western blots as a band doublet around the 120 kDa region (Kobia et al., 2014; Fig. 1E)

. We suspected that the slightly higher molecular weight band of the doublet may represent the N1ICD that is phosphorylated and destined for proteasomal degradation, while the lower molecular weight band represents newly generated N1ICD that has not been phosphorylated [43–45]. Indeed, in extracts of cells treated with the γ-secretase inhibitor DAPT to block the production of N1ICD, we observed the presence of the upper band only (Fig. 1E). To test if the upper band of the N1ICD doublet was indeed phosphorylated, we harvested proteins from unstimulated MCF10A cells, or from cells stimulated with EGTA for 10 minutes to induce N1ICD generation, or from cells stimulated with EGTA for 10 minutes and then returned to normal medium for 1.5 hours. We then treated the lysates with or without λ-phosphatase (λ-PPA) [46]. This analysis revealed that λ-PPA treatment resulted in a minor downshift of the N1ICD in extracts stimulated with EGTA for 10 minutes and in a large downshift in those in which the EGTA had been washed out for 1.5 hours after stimulation, indicating that N1ICD is progressively phosphorylated after S3 cleavage (Fig. 1F). Together, these data indicate that MCF10A cells are endowed with an endogenous pool of plasma membrane-localized NOTCH1 that can be canonically activated in a S2 and S3-dependent fashion to promote target gene transcription before being phosphorylated.

Dynamics of NOTCH1 receptor trafficking in MCF10A cells

To study the dynamics of endogenous NOTCH1 trafficking, we first treated MCF10A cells with the V-ATPase inhibitor BAfA1 for 4 hours to block lysosomal protein degradation. As previously observed [34], while most of NOTCH1 is localized to the plasma membrane (PM) in control-treated cells, most NOTCH1 accumulates in LAMP1-positive lysosomal compartments in BafA1-treated cells. A similar pattern of localization is observed for EGFR (Fig. 2A, quantified in A'). These data indicate that in unstimulated conditions endogenous NOTCH1 localization represents the steady state of a receptor that is continuously trafficked to lysosomes for degradation.

Because new synthesis of NOTCH1 is expected to compensate for its rapid lysosomal degradation, we studied NOTCH1 exocytic trafficking relative to EGFR. Consistent with continuous secretory trafficking of newly synthesized NOTCH1, we observe that in untreated cells an intracellular pool of NOTCH1 and EGFR colocalizes with the endoplasmic reticulum marker RTN3 (Reticulon-3; Fig. 2B). We reasoned that Ca^{2+} chelation, in addition to triggering shedding of the extracellular portion of Notch, when prolonged, is known to lead to exhaustion of the intracellular Ca^{2+} stores and membrane fusion arrest [47,48]. Indeed, 4 hours treatment with 2.5mM EGTA, results in clearing of the PM of existing NOTCH1 molecules and to accumulation of most NOTCH1 and EGFR in a RTN3-positive compartment (Fig. 2B; note that EGFR is still visible at the cell surface). This experiment highlights a strategy for controlling the release of NOTCH1 and tracking its trafficking to the PM.

To time endogenous NOTCH1 and EGFR trafficking from the ER to the cell surface, we washed out the EGTA-containing media after the 4 hour-treatment with fresh complete medium (w/o). We then subjected the cells to immunolabeling for NOTCH1, EGFR, and Giantin, a marker of the Golgi apparatus (GA). Interestingly, we observe that an intracellular pool of NOTCH1 and EGFR colocalizes with Giantin (Fig. 2C, quantified in C'). Treating the cells with EGTA for 4 hours caused accumulation of most NOTCH1, EGFR and Giantin in the ER, as well as alteration of Giantin localization. Strikingly, both NOTCH1 and EGFR almost exclusively localized in the GA upon 1 hour w/o, indicating that NOTCH1 and EGFR is rapidly resumed after EGTA w/o. Interestingly, EGFR presence, but not NOTCH1 presence is significantly increased on the PM 1 hour after EGTA w/o (Fig. 2C, quantified in C'), indicating that NOTCH1 trafficking to the PM is significantly slower than that of EGFR. A 4-hour w/o and overnight (ON) w/o fully restored NOTCH1 and EGFR localization to the cell surface, with localization quantitatively resembling or exceeding that of untreated cells (Fig. 2C, quantified in C'). Taken together, these data reveal time-resolved kinetics of NOTCH1 and EGFR secretion from the ER to the GA, and to the PM, and indicate that the bulk of the NOTCH1 pool progresses from the ER to GA and from GA to the

cell surface in less than 4 hours. This timeline is consistent with the timing of endocytic degradation obtained by limiting lysosomal activity with BafA1 treatment and indicates that in MCF10A cells NOTCH1 molecules possess an extremely limited lifespan of about 8 hours and are likely to reside on the cell surface only for a short time.

High-content screening identifies 51 novel potential modulators of intracellular NOTCH1 localization

The limited lifespan of endogenous NOTCH1 in MCF10A cells predicts that perturbation of genes that control NOTCH1 trafficking and signaling might significantly alter its steady state localization. Thus, we perturbed the activity of 2749 human genes with known or predicted small compound inhibitors belonging to different functional categories (see Supplemental file 1) in MCF10A cells. To this end, we reverse transfected cells on 10 arrayed plates containing individual pools of silencing RNAs (siRNA) targeting the human genes and controls (Fig. 3A). We subjected plates to EGTA stimulation or left them unstimulated, and then stained them with an antibody that recognizes the cytoplasmic portion of NOTCH1. The cells were counterstained with DAPI and phalloidin to visualize nuclei and cell cortices, respectively (Fig. 3B). We devised an automated high content image analysis pipeline to identify factors that when silenced affected NOTCH1 subcellular localization by altering receptor amounts on the cell surface, in the cytoplasm, or in the nucleus (Fig 3B). In such primary screen, we identified 231 potential modulators of NOTCH1 localization (Fig. 4A; Supplemental File 2). We then retested the positive hits using a custom-made plate containing 231 pools of esiRNA, a gene-silencing reagent comprised of a heterogeneous mixture of numerous siRNA targeting each gene [49] identified in the primary screen. This validation screen yielded 73 hits but only 51 of them confirmed the effects observed in the primary screen (Fig. 4B). Of these 51, the majority increased the intracellular pool of NOTCH1 either in unstimulated or in stimulated conditions (44/51), while a minority altered both PM and intracellular NOTCH1 (4/51) or increased nuclear NOTCH1 (3/51; Fig. 4C; Supplemental

File 3). Representative example of hits belonging to each phenotypic category are shown is Supplemental Fig. 1).

Modulation of NOTCH1 localization and signaling by *PTPN23*

Considering the role of endocytosis in regulation of Notch localization, to validate HCS hits, we began from *PTPN23*, one of the 8 identified genes that have been previously associated with regulation of endo-lysosomal trafficking (16% of the 51 hits: *CPA2, CTSE, MLC1, PIK3C2G, PTPN23, TINAGL1, ZNRF1, ZNRF2*). *PTPN23* encodes HD-PTP, a ubiquitous nonreceptor tyrosine pseudophosphatase that has been involved extensively in endosomal sorting, multivesicular body formation (MVB) and ESCRT activity [50,51]. Automated analysis of HCS IF images revealed that relative to control cells in which NOTCH1 mainly resided at the PM, *PTPN23* KD MCF10A cells exhibited marked intracellular NOTCH1 accumulation, which appeared as puncta (Supplemental Fig. 2A). We reasoned that *PTPN23* depletion might interfere with NOTCH1 endosomal trafficking or sorting. To identify the compartment in which the NOTCH1 accumulated, we co-stained cells with antibodies against NOTCH1 and the endo-lysosomal markers EEA1 or LAMP1, which identify early endosomes and lysosomes, respectively. Efficient depletion of *PTPN23* (Supplemental Fig. 2B) led to significant expansion of the cytoplasmic pool of puncta positive for EEA1, LAMP1, and NOTCH1 (Fig. 5A, quantified in A'). Quantitative analysis revealed that the NOTCH1 that accumulated upon *PTPN23* depletion mainly resided in puncta positive for EEA1 (Fig. 5A'). Taken together, these data indicated that *PTPN23* depletion might interfere with endosomal trafficking, thereby trapping NOTCH1 mostly in early endosomes.

We next evaluated how loss of *PTPN23* might affect Notch processing and signaling. Western blot analysis revealed a marked reduction of both N1FL and N1TM upon *PTPN23* KD (Fig. 5B) but surprisingly, the levels of N1ICD were not significantly altered, both in unstimulated and stimulated conditions (Fig. 5C). To assess the effect of *PTPN23* depletion on Notch signaling, we measured Notch-mediated RBPj-luc expression and found that when compared with control

cells, *PTPN23* silencing significantly suppressed Notch signaling in unstimulated conditions but not in the presence of EGTA (Fig. 5D). Similar observations were obtained when measuring *HES1* expression (Fig 5E). Because reduced biosynthetic N1FL levels could also result from low *NOTCH1* transcription, we measured *NOTCH1* mRNA levels by quantitative reverse transcription PCR (RT-qPCR) and found that upon *PTPN23* depletion, *NOTCH1* expression levels were mildly but significantly reduced (Fig 5H). These data indicate that *PTPN23* is required for NOTCH1 sorting into MVBs and for sustaining Notch expression and basal signaling and illustrate the screen's ability to identify novel modulators of NOTCH1 trafficking and signaling.

HCN2 silencing traps NOTCH1 in enlarged Golgi bodies and suppresses Notch signaling

Automated analysis of HCS IF images identified 4 genes encoding channels (*CACNB4, TRPM7, HCN2*, and *MLC1*) that upon KD in unstimulated conditions, caused cytosolic NOTCH1 accumulation (out of a total of 44 genes, a 9.1% enrichment; Supplemental file 3). Of these, *HCN2* KD led to the most striking phenotype, with strong NOTCH1 accumulation in the perinuclear space when compared with mock-silenced (non-targeting/NT) controls (Supplemental Fig. 3A). To test if NOTCH1 accumulated in the perinuclear GA, we knocked down *HCN2* (Supplemental Fig. 3B) and co-stained for NOTCH1 and the GA protein GIANTIN. Confocal analysis confirmed the perinuclear NOTCH1 localization observed in the HCS images and revealed increased localization of NOTCH1 in the GA, when compared to control cells (Fig. 6A, quantified in A'). Additionally, the analysis revealed that when compared with the control, *HCN2* silencing markedly reduced cell surface NOTCH1 levels (Fig 6A, quantified in A'), suggesting that HCN2 silencing might interfere with trafficking of newly made NOTCH1 to the cell surface. To assess this, we compared NOTCH1 and EGFR localization upon *HCN2* KD and 4-hour EGTA treatment. HCN2 silencing strongly accumulated NOTCH1 and EGFR in the GA. 4-hour EGTA treatment mildly but significantly increased the amount of NOTCH1 in the GA and reduced the amount of NOTCH1 and EGFR at the PM. However, both NOTCH1 and EGFR mostly failed to return to the PM after

1 or 4-hour w/o (Supplemental Fig. 4A; quantified in A'), indicating that both receptors do not traffic efficiently to the PM in the absence of HCN2. Relative to mock silencing, *HCN2* depletion markedly increased the volumes of the GA, nuclei, and cells, and led to loss of the TGN marker, TGN46 but not GOLGIN-97 (Fig 6B, quantified in B'). Collectively, these data indicated an unexpected role for HCN2 in organizing a functional TGN, competent for cargo secretion to the PM.

Next, we extended the analysis of *HCN2* KD to Notch signaling output. *HCN2* depletion significantly reduced expression of a Notch signaling reporter in unstimulated cells and limited the expression of the NOTCH1 target gene, *HES1*, relative to controls (Fig. 6C–D). Consistent with these observations, western blot analysis revealed that when compared with the control, *HCN2* silencing markedly reduced the levels of N1ICD both in the absence and presence of EGTA (Fig. 6E). Intriguingly, when compared with N1ICD expression upon *HCN2* silencing, Western blot analysis of the levels of the S1 substrate N1FL revealed the opposite trend, with *HCN2* KD elevating N1FL levels relative to the control (Fig. 6F; Supplemental Fig. 3D). In contrast, the levels of N1TM, the S2-processed form of NOTCH1, were reduced in *HCN2* KD cells, when compared with controls (Fig. 6F). Together, these findings indicate that HCN2 is required for NOTCH1 S1 processing and signaling. In the absence of *HCN2*, newly synthesized N1FL accumulates in the GA and is not efficiently trafficked to the cell membrane, resulting in reduced levels of the S2-(N1TM) and S3-processed (N1ICD) forms of NOTCH1.

SGK3 silencing elevates cytosolic NOTCH1 levels

Automated image analysis identified 5 kinases that when silenced, interfered with NOTCH1 localization (*DCK, EIF2AK1, MASTL, PIK3C2G, SGK3* (corresponding to 9.8% of 51 hits; Supplemental File 3). Of these, *SGK3* might regulate Notch receptor stability based on previous findings that SGK3 targets NDRG1 for FBW7-mediated proteasomal degradation [52], a process that also limits N1ICD stability [53]. Moreover, the SGK3 paralog, SGK1, has previously

been reported to negatively modulate Notch signaling by targeting NOTCH1 for proteasomal degradation [54]. Automated HCS image analysis revealed that relative to mock silencing, *SGK3* KD causes marked NOTCH1 accumulation in the cytosol (Supplemental Fig. 5A). To validate this observation, we silenced *SGK3* (Supplemental Fig. 5B–C) and analyzed the cells by confocal microscopy after co-staining with antibodies against GOLGIN-97, EEA1 and LAMP1, to mark the early TGN, early endosomes, and lysosomes, respectively. This analysis confirmed the presence of elevated intracellular NOTCH1 levels but revealed reduced colocalization with the GOLGIN-97- and EEA1-positive compartments (Fig. 7A, quantified in A'), whereas colocalization with the LAMP1-positive compartment did not differ significantly from the control (Fig. 7B, quantified in B').

Given the diffused accumulation of NOTCH1 observed upon *SGK3* silencing, we wondered whether this correlated with elevated NOTCH1 processing and signaling levels. We first tested which NOTCH1 form accumulated upon *SGK3* KD and found that *SGK3* depletion leads to elevated N1FL, N1TM, and N1ICD levels in both unstimulated and stimulated conditions (Fig. 7C–D). We next used the Notch signaling reporter cell line MCF10A-RbpJk-Luc and observed that when compared with the control, silencing *SGK3* caused significantly higher Notch signaling output upon EGTA stimulation (Fig. 7E). Although signaling did not differ significantly in unstimulated *SGK3*-silenced MCF10A-RbpJk-Luc cells when compared to mock silencing, RT-qPCR analysis revealed that *SGK3* KD in MCF10A cells significantly upregulated the expression of the Notch signaling targets *HEY1* and *NOTCH1,* but not HES1 (Fig. 7F–H).

The observation that depleting *SGK3* in MCF10A cells leads to elevated N1ICD levels made us wonder whether SGK3 is a negative modulator of NOTCH1 receptor stability and whether its reduction might impair NOTCH1 degradation. To test this possibility, we silenced *SGK3* and then treated the cells with cycloheximide (CHX) to block protein synthesis or with DMSO as a negative control. Because blocking the synthesis of new proteins would allow cells to turn over proteins that had been present before CHX addition, we reasoned that if SGK3 is required for efficient NOTCH1 degradation, upon CHX treatment *SGK3*-depleted cells would

exhibit elevated NOTCH1 levels, when compared with control cells. Western blot analysis using antibodies against N1FL and N1ICD revealed that *SGK3* silencing caused marked increase in the levels of N1FL and N1ICD, when compared with control. However, N1FL and N1ICD levels were markedly decreased in both control and *SGK3* KD cells upon CHX treatment (Fig. 7I), indicating that SGK3 is not required for NOTCH1 destabilization. Finally, to assess whether SGK3 contributed directly or indirectly to N1ICD phosphorylation, we silenced *SGK3* in MCF10A cells and then performed the λ-PPA assay. This analysis revealed that in *SGK3* KD cells, accumulated N1ICD was still phosphorylated, and that phosphorylation could be erased by extract treatment with λ-PPA (Fig. 7J), indicating that SGK3 is not required for N1ICD phosphorylation. Taken together, these data indicate that SGK3 negatively regulates NOTCH1 levels and signaling indirectly by a mechanism other than control of NOTCH1 stability and/or degradation.

Pharmacologic SGK3 inhibition elevates N1ICD levels and Notch signaling

To explore whether SGK3 modulation of NOTCH1 could be controlled pharmacologically, we examined the effect of VPS34-IN1, a well characterized SGK3 inhibitor [55,56]. We first tested if VPS34-IN1 can effectively block SGK3 activity in MCF10A cells. Because we were unable to directly evaluate SGK3 phosphorylation upon treatment of cultured cells with VPS34-IN1, we evaluated the phosphorylation levels of NDRG1, a known SGK3 substrate [52,57]. SGK3 can be activated by stimulating the cells with growth factors, such as IGF1 and EGF [58–60]. Thus, we stimulated control or VPS34-IN1-treated cells with EGF to promote NDRG1 phosphorylation. Strikingly, EGF failed to elicit NDRG1 phosphorylation in VPS34-IN1-treated cells and erased the basal low level of NDRG1 phosphorylation in unstimulated cells (Fig 8A), indicating that treatment with VPS34-IN1 potently blocks SGK3 activity in cultured MCF10A cells.

Next, to determine if pharmacologic VPS34-IN1 treatment reproduces the effects of *SGK3* silencing on NOTCH1, we treated MCF10A cells with VPS34-IN1 and measured N1ICD levels. Western blot analysis revealed that relative to mock treatment, VPS34-IN1 significantly elevated

the levels of N1ICD (Fig 8B). To establish whether VPS34-IN1 treatment also elevates Notch targets, we examined the expression levels of *HEY1* by RT-qPCR. This analysis revealed that when compared with control cells, *HEY1* levels were significantly higher in VPS34-IN1-treated cells (Fig. 8C). Taken together, these data indicate that as with *SGK3* silencing, pharmacologic VPS34-IN1 treatment elevates NOTCH1 levels and promotes Notch signaling.

A secondary screen using a Notch reporter identifies 39 new modulators of NOTCH1 localization that affect signaling output

To systematically determine the impact of the modulators of NOTCH1 trafficking on Notch signaling, we individually silenced with esiRNA the 231 primary hits in MCF10A-RbpJk-Luc cells with or without EGTA stimulation and measured signaling output. We included *PTPN23* and *SGK3* as positive controls since their positive contribution to unstimulated signaling and negative contribution to stimulated signaling had already been assessed. As expected, *PTPN23* and *SGK3* depletion reproduced previous evidence. Focusing on the validated 51 genes that affect localization in the secondary screen, the analysis identified 39 depletions (76.5% of the total) that altered Notch signaling by at least 30%, with 21 modulating signaling in unstimulated conditions only, 8 in stimulated conditions only, and 10 in both conditions (Fig. 9A–C; Supplemental File 3). Of the 39 depletions, 30 led to reduced signaling (9 of which also in stimulated conditions), while 9 led to increased signaling (8 of which in stimulated conditions (Fig 9D). NOTCH1 phenotypic classes of the 39 depletions are reported in Fig. 9D, while information about signaling modulation by the set of 231 siRNA of the primary screen is included in Supplemental File 2. This approach led to the identification of several new positive and negative regulators of Notch signaling that require further characterization.

Discussion

NOTCH1 activity in MCF10A cells has been mostly characterized using transfection of activated forms [61,62]. Here we have shown that it is possible to activate endogenous NOTCH1 using a short pulse of Ca^{2+} chelation that destabilizes the NOTCH1 HD domain leading to S2 and S3 cleavage, as previously reported for a variety of different cell types [6,63–65]. Interestingly, we find that MCF10A possess a low level basal S3 cleavage and that, upon S3 cleavage NOTCH1 is rapidly phosphorylated, an event that have been described to lead to proteasomal degradation of NICD. Whether such basal S3 cleavage depends on transactivation among neighboring cells, considering that MCF10A express also NOTCH1 ligands [34], or whether it is a cell autonomous occurrence due to intracellular ligand-dependent activation remains to be determined.

By means of inhibition of lysosomal degradation, we also have determined that trafficking of NOTCH1 occurs similarly to what has been reported in other epithelial systems, such as *in vivo* in imaginal discs of *Drosophila* [66]. Interestingly, upon inhibition of lysosomal degradation, NOTCH1 not only accumulates in lysosomes but is also depleted from the PM, suggesting that some coordination of new synthesis and/or ER to PM trafficking with clearance might exist. Kinetics of transit indicate that NOTCH1 traffics from the ER to the GA in less than 1 hour and from the GA to PM in less than 3 hours. These times indicate that on average the half-life of each NOTCH1 molecule is only approximately 4 hours, a time comparable to previous *in vivo* findings using *Drosophila* Notch [67]. Such half-life is also compatible with the two main events described during NOTCH1 secretion, namely receptor glycosylation and S1 cleavage executed by Furin [68,69].

Because the half-life of NOTCH1 is very limited, we posited that genetic perturbations could result in visible changes in steady-state endogenous NOTCH1 localization. Such possibility suggested that high throughput determination of steady-state NOTCH1 localization could uncover new genes that are important for NOTCH1 localization and associated event of activation, as well as new genes that regulate trafficking in MCF10A cells. We identified 51 such genes by high

content screening and secondary validation with an alternative set of reagents to exclude the possibility of off target or nonspecific effects. Most of the identified genes are expressed in MCF10A cells according to recent RNAseq analyses [70,71]. While some of the candidate genes, especially those obtained upon EGTA stimulation, might be the result of indirect or combined effects with transient extracellular Ca^{2+} depletion, 31, the vast majority, have been identified in unstimulated conditions, indicating that tight NOTCH1 trafficking regulation is crucial to determine basal levels of signaling. Interestingly, among these 31 basal signaling genes, 30 are required to promote RbpJk transcriptional activity, while only *CALM2* appeared to negatively regulate signaling. These data suggest that sustaining high NOTCH1 turnover enables basal signaling. Also, all 3 genes that we have best characterized alter the distribution of markers of trafficking compartments, indicating that the effect on NOTCH1 trafficking and signaling of the identified candidate genes is likely to be indirect.

Several phenotype-based genome-wide Notch screens have been performed *in vivo*, in animal models such as *Drosophila* [72–75] and in cellular systems [76,77]. Strikingly, paralogs of 12 genes out of the 51 that we have identified have been previously identified as modulators of Notch phenotypes in previous screens (*CACNB4, CALM2, CIB2, CMPK1*, *CTSE, MAP3K12, PIK3K2CG, PTPN23, TRPM7, USP36, UFD1L, ZNRF1*), suggesting that ours is a robust strategy and that some of the candidates might play a conserved function and might be validated in *in vivo* models.

Among genes that we have identified, some have previously been associated with regulation of the mTOR pathway (*CIB2, MASTL, MC1R, SGK3, ZNRF1, ZNRF2*). ZNRF1 appears to be required for EGFR sorting to late endosomes, a prerequisite for lysosomal degradation and signaling termination [78]. In contrast, ZNRF2 has been found to regulate mTOR signaling at lysosomes [79]. Also, the calcium and integrin binding protein 2 encoded by the gene *CIB2*, which we found here as a negative regulator of NOTCH1, is a negative regulator of mTOR signaling in the mouse retinal pigmented epithelium [80]. Similarly, the MASTL kinase regulates mTOR [81]

and EGFR [82]. Finally, as a NOTCH1 modulator we have found MC1R (Melacortin 1 receptor), which in melanocytes contributes to pigmentation by regulating the TFEB paralog MITF, among other pathways. Interestingly, agonists of MC1R are reported to modulate Notch signaling in synovial fibroblast in models of arthritis [83], suggesting that coregulation of Notch and the MC1R/MITF pathway might exist.

We have characterized the activity of *SGK3* as a negative regulator of NOTCH1 expression and signaling. *SGK3* encodes a PI3K-dependent endosome-localized serine/threonine kinase with similar substrate specificity to AKT, a kinase acting upstream of mTOR widely involved in tumorigenesis [83]. All forms of NOTCH1 accumulate in *SGK3* depleted cells and we have excluded that SGK3 directly phosphorylates N1ICD. Thus, SGK3 is likely to act indirectly on NOTCH1. Because SGK3 has been proposed to promote mTOR activation in endo-lysosomal compartments, one interesting possibility is that mTOR and NOTCH1 might be alternatively regulated. Interestingly, resistance to mTOR inhibition in breast cancer cells is mediated by hVPS34 and SGK3, defining an AKT independent mTOR activation pathway [84]. Considering that inhibition of Notch activity on TNBCC abrogates *SGK3* expression [85], a Notch/SGK3 regulatory loop might exist in breast cells, that will be further investigated in future. Finally, it will be important to test whether SGK3 acts as a negative regulator in contexts in which NOTCH1 acts as a tumor suppressor, such as during skin tumorigenesis [86].

The relocalization of NOTCH1 to early endosomes upon *PTPN23* KD matches earlier observations in human cells that indicate that PTPN23 resides on early endosomes and that its depletion causes EGFR accumulation in EEA1-positive endosomes [87]. The activity of PTPN23 on endocytic trafficking and ESCRT function is well documented [50,88,89]. However, we find that NOTCH1 signaling activity upon *PTPN23* KD is slightly reduced, yet the loss of ESCRT components usually enhances Notch signaling [31,33,66,90]. Considering that *PTPN23* has been described as a tumor suppressor as is the case of ESCRT genes, and that loss of PTPN23 contributes to mammary tumorigenesis by altering endocytic trafficking of cancer-relevant

cargoes [91,92], it will be important in the future to understand whether Notch alteration contributes to tumorigenesis initiated by loss of *PTPN23* in contexts in which Notch acts as a tumor suppressor, as well as to further dissect the mechanistic relationship between Notch and PTPN23.

In addition to *PTPN23* and *SGK3,* five other identified genes have been associated with breast tumorigenesis (*GPCR, GPR125, MET, NUDT5, TINAGL1*). In fact, the gastrin-releasing peptide receptor, a G protein couple receptor (GPCR) encoded by *GRPR* is an established marker of prostate and breast cancers [93,94]. Loss of *TINAGL1* encoding the tubulointerstitial nephritis antigen-like 1, a secreted basement membrane inactive peptidase, has been found as a marker for poor prognosis in breast cancer [95] and appears to negatively regulate Integrin and EGFR signaling in triple negative breast cancer [96]. In addition, the NUDIX hydrolase type 5 encoded by *NUDT5* is an ADP-ribose pyrophosphatase and nucleotide metabolizing enzyme involved in regulation of AKT in breast cancer [97]. It generates nuclear ATP to fuel chromatin remodeling, gene expression, and proliferation [98]. Also, *GPR125* encodes a GPCR that regulates epithelial polarity [99] and is associated with poor outcome in breast cancer [100]. Finally, *MET,* which encodes the hepatocyte growth factor receptor (HGFR), is a proto-oncogenic receptor tyrosine kinase found to be coregulated with Notch in physiologic as well as several pathologic conditions, including in gastric and breast cancer cells [101–105]. These combined studies warrant further characterization of the identified candidate genes in breast cancer cells.

A few genes that we have isolated in the screen have been previously involved in regulation of Notch signaling (*ADORA1, CALM2, JAK3, MAP3K12, PLAU, TRPM7*). Inhibition of adenosine A1 receptor encoded by *ADORA1* has been recently implicated in Notch dependent signaling in lung cancer cells [106]. Also, Notch signaling activation triggers JAK3 ubiquitination and degradation [107]. In addition, Notch1 activates *PLAU* encoding the urokinase-type plasminogen activator, a secreted ECM enzyme, in migrating mouse keratinocytes [108].

Some of the identified genes that have previously been associated with Notch signaling appear connected with cation regulation, even if we identified the vast majority in unstimulated conditions (*CALM2, HCN2, MAP3K12, TRPM7*). A case in point is that of *TRPM7,* encoding the transient receptor potential melastatin-related 7, a divalent Ca^{2+} and Mg^{2+} channel fused with a functional serine/threonine-protein kinase that is widely overexpressed in breast cancer (reviewed by [109]. Remarkably, *TRPM7* has been described as a potent inducer of Notch activation during glial tumorigenesis [110,111]. Intriguingly, Mg^{2+} supplementation during osteogenesis appears to activate Notch1 signaling, a phenomenon reverted by TRPM7 inhibition [112]. In addition, the *Caenorhabditis elegans* homolog of MAP3K12 (also called DLK), a Ca^{2+} activated MAP kinase involved in trafficking and signaling regulation that we identified [113,114], has been shown to repress Notch signaling by activating autophagy in neurons [115]. Finally, we have the calmodulin-encoding *CALM2.* CALM2 and CaMKIV activity have been reported to enhance Notch1 activity in osteoclasts and prostate cancer cells [116,117], while calmodulin-dependent serine protein kinase (CASK) does that in pancreatic cancer cells [118], and cardiovascular development [119]. This evidence suggests that changes in intracellular cation regulation might fine tune extracellular and/or luminal Notch activation.

Our observation that expression of *HCN2* encoding the hyperpolarization-activated cyclic nucleotide-gated channel 2 in MCF10A is required to support post-GA trafficking of NOTCH1 as well as its S1 cleavage suggest that inhibition of HCN2 might reduce the oncogenic effects of NOTCH1 when mutations are not liberating it from membranes. We observed a major alteration of GA and TGN morphology upon *HCN2* depletion in MCF10A cells. This suggest that GA trafficking to the TGN might be supported by HCN2, thus leading to correct Furin cleavage of NOTCH1. Importantly, recent data indicate that HCN2 is expressed in MCF10A cells and that it is overexpressed in triple negative breast cancer cells. In the latter, inhibition or depletion of HCN2 leads to misregulation of intracellular Ca^{2+} regulation and ER stress [120]. This evidence suggests

that analysis of HCN2 inactivation in breast cancer, in particular the triple negative type that is defined by elevated Notch activity (reviewed in [121]), could be beneficial.

In addition to these genes, we also identified as modifiers two genes that encode the deubiquitinating enzymes (DUBs) USP36 and USP39. Silencing both leads to intracellular accumulation of NOTCH1. However, *USP36* appears to promote signaling, while *USP39* represses it. USP39 does not possesses deubiquitinating activity and is present in the nucleus as a splicing factor [122,123] and has been found to be in complex with the γ-secretase component, Nicastrin, in large-scale proteomics of human cells [124]. USP36 is nucleolar and is involved in ribosome biogenesis [125,126]. In contrast, in flies, USP36 represses autophagy [127] and has been shown to control H2B ubiquitination and chromatin regulation leading to repression of Notch signaling [128]. This evidence suggest that these DUBs could be involved in conserved network of Notch signaling regulation occurring in the nucleus.

Overall, the genes isolated in our screen expand the repertoire of genes regulating intracellular trafficking and NOTCH1 localization. They also represent potential new drug targets possibly relevant to breast tumorigenesis and other Notch-associated pathologies.

References

1. Artavanis-Tsakonas S, Rand MD, Lake RJ, Artavanis-Tsakonas S, Rand MD, Lake RJ. Notch signaling: cell fate control and signal integration in development. Science. 1999;284: 770–776. doi:10.1126/science.284.5415.770
2. Andersson ER, Sandberg R, Lendahl U. Notch signaling: simplicity in design, versatility in function. Development. 2011;138: 3593–612. doi:10.1242/dev.063610
3. Koch U, Lehal R, Radtke F. Stem cells living with a Notch. Development. 2013;140: 689–704. doi:10.1242/dev.080614
4. Mašek J, Andersson ER. The developmental biology of genetic Notch disorders. Development. 2017;144: 1743–1763. doi:10.1242/DEV.148007
5. Blaumueller CM, Qi H, Zagouras P, Artavanis-Tsakonas S. Intracellular Cleavage of Notch Leads to a Heterodimeric Receptor on the Plasma Membrane. Cell. 1997;90: 281–291. doi:10.1016/S0092-8674(00)80336-0

6. Rand MD, Grimm LM, Artavanis-Tsakonas S, Patriub V, Blacklow SC, Sklar J, et al. Calcium depletion dissociates and activates heterodimeric notch receptors. Mol Cell Biol. 2000;20: 1825–35. Available: http://www.ncbi.nlm.nih.gov/pubmed/10669757

7. Kopan R, Ilagan MXG. The Canonical Notch Signaling Pathway: Unfolding the Activation Mechanism. Cell. 2009;137: 216–233. doi:10.1016/j.cell.2009.03.045

8. van Tetering G, van Diest P, Verlaan I, van der Wall E, Kopan R, Vooijs M. Metalloprotease ADAM10 is required for Notch1 site 2 cleavage. Journal of Biological Chemistry. 2009;284: 31018–31027. doi:10.1074/jbc.M109.006775

9. Herreman A, Serneels L, Annaert W, Collen D, Schoonjans L, de Strooper B. Total inactivation of gamma-secretase activity in presenilin-deficient embryonic stem cells. Nat Cell Biol. 2000;2: 461–2. doi:10.1038/35017105

10. Schroeter EH, Kisslinger JA, Kopan R. Notch-1 signalling requires ligand-induced proteolytic release of intracellular domain. Nature. 1998;393: 382–6. doi:10.1038/30756

11. Zhang Z, Nadeau P, Song W, Donoviel D, Yuan M, Bernstein A, et al. Presenilins are required for gamma-secretase cleavage of beta-APP and transmembrane cleavage of Notch-1. Nat Cell Biol. 2000;2: 463–5. doi:10.1038/35017108

12. Bray SJ. Notch signalling: a simple pathway becomes complex. Nat Rev Mol Cell Biol. 2006;7: 678–89. doi:10.1038/nrm2009

13. Tagami S, Okochi M, Yanagida K, Ikuta A, Fukumori A, Matsumoto N, et al. Regulation of Notch signaling by dynamic changes in the precision of S3 cleavage of Notch-1. Mol Cell Biol. 2008;28: 165–76. doi:10.1128/MCB.00863-07

14. Hori K, Sen A, Kirchhausen T, Artavanis-Tsakonas S. Regulation of ligand-independent Notch signal through intracellular trafficking. Commun Integr Biol. 2012;5: 374–6. doi:10.4161/cib.19995

15. Fortini ME, Bilder D. Endocytic regulation of Notch signaling. Curr Opin Genet Dev. 2009;19: 323–8. doi:10.1016/j.gde.2009.04.005

16. Moretti J, Brou C. Ubiquitinations in the notch signaling pathway. Int J Mol Sci. 2013;14: 6359–81. doi:10.3390/ijms14036359

17. Sakata T, Sakaguchi H, Tsuda L, Higashitani A, Aigaki T, Matsuno K, et al. Drosophila Nedd4 regulates endocytosis of notch and suppresses its ligand-independent activation. Curr Biol. 2004;14: 2228–36. doi:10.1016/j.cub.2004.12.028

18. Schneider M, Troost T, Grawe F, Martinez-Arias A, Klein T. Activation of Notch in lgd mutant cells requires the fusion of late endosomes with the lysosome. J Cell Sci. 2013;126: 645–56. doi:10.1242/jcs.116590

19. Panin VM, Papayannopoulos V, Wilson R, Irvine KD. Fringe modulates Notch-ligand interactions. Nature. 1997;387: 908–912. doi:10.1038/43191

20. Acar M, Jafar-Nejad H, Takeuchi H, Rajan A, Ibrani D, Rana NA, et al. Rumi is a CAP10 domain glycosyltransferase that modifies Notch and is required for Notch signaling. Cell. 2008;132: 247–258. doi:10.1016/J.CELL.2007.12.016

21. Shi S, Stanley P. Protein O-fucosyltransferase 1 is an essential component of Notch signaling pathways. Proc Natl Acad Sci U S A. 2003;100: 5234–5239. doi:10.1073/PNAS.0831126100

22. Seugnet L, Simpson P, Haenlin M. Requirement for dynamin during Notch signaling in Drosophila neurogenesis. Dev Biol. 1997;192: 585–598. doi:10.1006/dbio.1997.8723

23. Xu T, Artavanis-Tsakonas S. deltex, a locus interacting with the neurogenic genes, Notch, Delta and mastermind in Drosophila melanogaster. Genetics. 1990;126: 665–77. Available: http://www.pubmedcentral.nih.gov/articlerender.fcgi?artid=1204222&tool=pmcentrez&rendertype=abstract

24. Matsuno K, Diederich RJ, Go MJ, Blaumueller CM, Artavanis-Tsakonas S. Deltex acts as a positive regulator of Notch signaling through interactions with the Notch ankyrin repeats. Development. 1995;121: 2633–44. Available: http://www.ncbi.nlm.nih.gov/pubmed/7671825

25. Diederich RJ, Matsuno K, Hing H, Artavanis-Tsakonas S. Cytosolic interaction between deltex and Notch ankyrin repeats implicates deltex in the Notch signaling pathway. Development. 1994;120: 473–81. Available: http://www.ncbi.nlm.nih.gov/pubmed/8162848

26. Kishi N, Tang Z, Maeda Y, Hirai A, Mo R, Ito M, et al. Murine homologs of deltex define a novel gene family involved in vertebrate Notch signaling and neurogenesis. International Journal of Developmental Neuroscience. 2001;19: 21–35. doi:10.1016/S0736-5748(00)00071-X

27. Hori K, Fostier M, Ito M, Fuwa TJ, Go MJ, Okano H, et al. Drosophila deltex mediates suppressor of Hairless-independent and late-endosomal activation of Notch signaling. Development. 2004;131: 5527–37. doi:10.1242/dev.01448

28. Cornell M, Evans DA, Mann R, Fostier M, Flasza M, Monthatong M, et al. The Drosophila melanogaster Suppressor of deltex gene, a regulator of the Notch receptor signaling pathway, is an E3 class ubiquitin ligase. Genetics. 1999;152: 567–76. Available: http://www.pubmedcentral.nih.gov/articlerender.fcgi?artid=1460625&tool=pmcentrez&rendertype=abstract

29. Chastagner P, Israël A, Brou C, Chastagner P, Israe A, Israël A, et al. AIP4/Itch regulates Notch receptor degradation in the absence of ligand. Wölfl S, editor. PLoS One. 2008;3: e2735. doi:10.1371/journal.pone.0002735

30. Wilkin MB, Carbery A-M, Fostier M, Aslam H, Mazaleyrat SL, Higgs J, et al. Regulation of Notch Endosomal Sorting and Signaling by Drosophila Nedd4 Family Proteins. Current Biology. 2004;14: 2237–2244. doi:10.1016/j.cub.2004.11.030

31. Vaccari T, Bilder D. The Drosophila tumor suppressor vps25 prevents nonautonomous overproliferation by regulating notch trafficking. Dev Cell. 2005;9: 687–98. doi:10.1016/j.devcel.2005.09.019

32. Hori K, Sen A, Kirchhausen T, Artavanis-Tsakonas S. Synergy between the ESCRT-III complex and Deltex defines a ligand-independent Notch signal. J Cell Biol. 2011;195: 1005–15. doi:10.1083/jcb.201104146

33. Thompson BJ, Mathieu J, Sung H-H, Loeser E, Rørth P, Cohen SM. Tumor suppressor properties of the ESCRT-II complex component Vps25 in Drosophila. Dev Cell. 2005;9: 711–20. doi:10.1016/j.devcel.2005.09.020

34. Kobia F, Duchi S, Deflorian G, Vaccari T. Pharmacologic inhibition of vacuolar H+ ATPase reduces physiologic and oncogenic Notch signaling. Mol Oncol. 2014;8: 207–20. doi:10.1016/j.molonc.2013.11.002

35. Kozik P, Hodson N a, Sahlender DA, Simecek N, Soromani C, Wu J, et al. A human genome-wide screen for regulators of clathrin-coated vesicle formation reveals an unexpected role for the V-ATPase. Nat Cell Biol. 2013;15: 50–60. doi:10.1038/ncb2652

36. Yan Y, Denef N, Schüpbach T, Schu T, Schüpbach T. The Vacuolar Proton Pump, V-ATPase, Is Required for Notch Signaling and Endosomal Trafficking in Drosophila. Dev Cell. 2009;17: 387–402. doi:10.1016/j.devcel.2009.07.001

37. Lange C, Prenninger S, Knuckles P, Taylor V, Levin M, Calegari F. The H(+) vacuolar ATPase maintains neural stem cells in the developing mouse cortex. Stem Cells Dev. 2011;20: 843–50. doi:10.1089/scd.2010.0484

38. Sethi N, Yan Y, Quek D, Schupbach T, Kang Y. Rabconnectin-3 is a functional regulator of mammalian notch signaling. Journal of Biological Chemistry. 2010;285: 34757–34764. doi:10.1074/jbc.M110.158634

39. Vaccari T, Duchi S, Cortese K, Tacchetti C, Bilder D. The vacuolar ATPase is required for physiological as well as pathological activation of the Notch receptor. Development. 2010;137: 1825–1832. doi:10.1242/dev.045484

40. Valapala M, Hose S, Gongora C, Dong L, Wawrousek EF, Samuel Zigler J, et al. Impaired endolysosomal function disrupts Notch signalling in optic nerve astrocytes. Nat Commun. 2013;4: 1629. doi:10.1038/ncomms2624

41. Birmingham A, Selfors LM, Forster T, Wrobel D, Kennedy CJ, Shanks E, et al. Statistical methods for analysis of high-throughput RNA interference screens. Nat Methods. 2009;6: 569–75. doi:10.1038/nmeth.1351

42. Soule HD, Maloney TM, Wolman SR, Peterson WD, Brenz R, McGrath CM, et al. Isolation and characterization of a spontaneously immortalized human breast epithelial cell line, MCF-10. Cancer Res. 1990;50: 6075–86. Available: http://www.ncbi.nlm.nih.gov/pubmed/1975513

43. Fryer CJ, White JB, Jones KA. Mastermind recruits CycC:CDK8 to phosphorylate the Notch ICD and coordinate activation with turnover. Mol Cell. 2004;16: 509–520. doi:10.1016/j.molcel.2004.10.014

44. Morrugares R, Correa-Sáez A, Moreno R, Garrido-Rodríguez M, Muñoz E, de la Vega L, et al. Phosphorylation-dependent regulation of the NOTCH1 intracellular domain by dual-specificity tyrosine-regulated kinase 2. Cellular and Molecular Life Sciences. 2020;77: 2621. doi:10.1007/S00018-019-03309-9

45. Li N, Fassl A, Chick J, Inuzuka H, Li X, Mansour MR, et al. Cyclin C is a haploinsufficient tumor suppressor. Nat Cell Biol. 2014;16: 1080. doi:10.1038/NCB3046

46. Satinover DL, Leach CA, Stukenberg PT, Brautigan DL. Activation of Aurora-A kinase by protein phosphatase inhibitor-2, a bifunctional signaling protein. Proc Natl Acad Sci U S A. 2004;101: 8625. doi:10.1073/PNAS.0402966101

47. Hay JC. Calcium: A fundamental regulator of intracellular membrane fusion? EMBO Reports. European Molecular Biology Organization; 2007. pp. 236–240. doi:10.1038/sj.embor.7400921

48. Pryor PR, Mullock BM, Bright NA, Gray SR, Luzio JP. The role of intraorganellar Ca2+ in late endosome-lysosome heterotypic fusion and in the reformation of lysosomes from hybrid organelles. Journal of Cell Biology. 2000;149: 1053–1062. doi:10.1083/jcb.149.5.1053

49. Theis M, Buchholz F. MISSION esiRNA for RNAi screening in mammalian cells. Journal of Visualized Experiments. 2010 [cited 24 Mar 2021]. doi:10.3791/2008

50. Doyotte A, Mironov A, McKenzie E, Woodman P. The Bro1-related protein HD-PTP/PTPN23 is required for endosomal cargo sorting and multivesicular body morphogenesis. Proc Natl Acad Sci U S A. 2008;105: 6308. doi:10.1073/PNAS.0707601105

51. Tabernero L, Woodman P. Dissecting the role of His domain protein tyrosine phosphatase/PTPN23 and ESCRTs in sorting activated epidermal growth factor receptor to the multivesicular body. Biochemical Society Transactions. Portland Press Ltd; 2018. pp. 1037–1046. doi:10.1042/BST20170443

52. Gasser JA, Inuzuka H, Lau AW, Wei W, Beroukhim R, Toker A. SGK3 Mediates INPP4B-Dependent PI3K Signaling in Breast Cancer. Mol Cell. 2014;56: 595–607. doi:10.1016/j.molcel.2014.09.023

53. Oberg C, Li J, Pauley A, Wolf E, Gurney M, Lendahl U. The Notch Intracellular Domain Is Ubiquitinated and Negatively Regulated by the Mammalian Sel-10 Homolog. Journal of Biological Chemistry. 2001;276: 35847–35853. doi:10.1074/jbc.M103992200

54. Mo JS, Ann EJ, Yoon JH, Jung J, Choi YH, Kim HY, et al. Serum- and glucocorticoid-inducible kinase 1 (SGK1) controls notch1 signaling by downregulation of protein stability through Fbw7 ubiquitin ligase. J Cell Sci. 2011;124: 100–112. doi:10.1242/jcs.073924

55. Bago R, Malik N, Munson MJ, Prescott AR, Davies P, Sommer E, et al. Characterization of VPS34-IN1, a selective inhibitor of Vps34, reveals that the phosphatidylinositol 3-phosphate-binding SGK3 protein kinase is a downstream target of class III phosphoinositide 3-kinase. Biochemical Journal. 2014;463: 413–427. doi:10.1042/BJ20140889

56. Ronan B, Flamand O, Vescovi L, Dureuil C, Durand L, Fassy F, et al. A highly potent and selective Vps34 inhibitor alters vesicle trafficking and autophagy. Nat Chem Biol. 2014;10: 1013–1019. doi:10.1038/nchembio.1681

57. Tovell H, Testa A, Zhou H, Shpiro N, Crafter C, Ciulli A, et al. Design and Characterization of SGK3-PROTAC1, an Isoform Specific SGK3 Kinase PROTAC Degrader. ACS Chem Biol. 2019;14: 2024–2034. doi:10.1021/acschembio.9b00505

58. Kobayashi T, Deak M, Morrice N, Cohen P. Characterization of the structure and regulation of two novel isoforms of serum- and glucocorticoid-induced protein kinase. Biochemical Journal. 1999;344: 189–197. doi:10.1042/0264-6021:3440189

59. Virbasius J v., Song X, Pomerleau DP, Zhan Y, Zhou GW, Czech MP. Activation of the Akt-related cytokine-independent survival kinase requires interaction of its phox domain with endosomal phosphatidylinositol 3-phosphate. Proc Natl Acad Sci U S A. 2001;98: 12908–12913. doi:10.1073/pnas.221352898

60. Malik N, Macartney T, Hornberger A, Anderson KE, Tovell H, Prescott AR, et al. Mechanism of activation of SGK3 by growth factors via the Class 1 and Class 3 PI3Ks. Biochemical Journal. 2018;475: 117–135. doi:10.1042/BCJ20170650

61. Mazzone M, Selfors LM, Albeck J, Overholtzer M, Sale S, Carroll DL, et al. Dose-dependent induction of distinct phenotypic responses to Notch pathway activation in mammary epithelial cells. Proc Natl Acad Sci U S A. 2010;107: 5012–5017. doi:10.1073/PNAS.1000896107

62. Meurette O, Stylianou S, Rock R, Collu GM, Gilmore AP, Brennan K. Notch activation induces Akt signaling via an autocrine loop to prevent apoptosis in breast epithelial cells. Cancer Res. 2009;69: 5015–22. doi:10.1158/0008-5472.CAN-08-3478

63. Tremblay I, Paré E, Arsenault D, Douziech M, Boucher MJ. The MEK/ERK Pathway Promotes NOTCH Signalling in Pancreatic Cancer Cells. PLoS One. 2013;8: 85502. doi:10.1371/JOURNAL.PONE.0085502

64. Swaminathan B, Youn SW, Naiche LA, Du J, Villa SR, Metz JB, et al. Endothelial Notch signaling directly regulates the small GTPase RND1 to facilitate Notch suppression of endothelial migration. Scientific Reports 2022 12:1. 2022;12: 1–14. doi:10.1038/s41598-022-05666-1

65. Westhoff B, Colaluca IN, D'Ario G, Donzelli M, Tosoni D, Volorio S, et al. Alterations of the Notch pathway in lung cancer. Proc Natl Acad Sci U S A. 2009;106: 22293–22298. doi:10.1073/PNAS.0907781106/SUPPL_FILE/0907781106SI.PDF

66. Vaccari T, Lu H, Kanwar R, Fortini ME, Bilder D. Endosomal entry regulates Notch receptor activation in Drosophila melanogaster. J Cell Biol. 2008;180: 755–62. doi:10.1083/jcb.200708127

67. Couturier L, Trylinski M, Mazouni K, Darnet L, Schweisguth F. A fluorescent tagging approach in Drosophila reveals late endosomal trafficking of Notch and Sanpodo. J Cell Biol. 2014;207: 351. doi:10.1083/JCB.201407071

68. Sasamura T, Ishikawa HO, Sasaki N, Higashi S, Kanal M, Nakao S, et al. The O-fucosyltransferase O-fut1 is an extracellular component that is essential for the constitutive endocytic trafficking of Notch in Drosophila. Development. 2007;134: 1347–1356. doi:10.1242/DEV.02811

69. Logeat F, Bessia C, Brou C, LeBail O, Jarriault S, Seidah NG, et al. The Notch1 receptor is cleaved constitutively by a furin-like convertase. Proc Natl Acad Sci U S A. 1998;95: 8108–8112. doi:10.1073/PNAS.95.14.8108

70. Goh JJH, Goh CJH, Lim QW, Zhang S, Koh CG, Chiam KH. Transcriptomics indicate nuclear division and cell adhesion not recapitulated in MCF7 and MCF10A compared to luminal A breast tumours. Scientific Reports 2022 12:1. 2022;12: 1–17. doi:10.1038/s41598-022-24511-z

71. Gross SM, Dane MA, Smith RL, Devlin KL, McLean IC, Derrick DS, et al. A multi-omic analysis of MCF10A cells provides a resource for integrative assessment of ligand-mediated molecular and phenotypic responses. Communications Biology 2022 5:1. 2022;5: 1–20. doi:10.1038/s42003-022-03975-9

72. Saj A, Arziman Z, Stempfle D, van Belle W, Sauder U, Horn T, et al. A combined ex vivo and in vivo RNAi screen for Notch regulators in Drosophila reveals an extensive Notch interaction network. Dev Cell. 2010;18: 862–876. doi:10.1016/j.devcel.2010.03.013

73. Mummery-Widmer JL, Yamazaki M, Stoeger T, Novatchkova M, Bhalerao S, Chen D, et al. Genome-wide analysis of Notch signalling in Drosophila by transgenic RNAi. Nature. 2009;458: 987–992. doi:10.1038/nature07936

74. Kankel MW, Hurlbut GD, Upadhyay G, Yajnik V, Yedvobnick B, Artavanis-tsakonas S. Investigating the Genetic Circuitry of Mastermind in Drosophila, a Notch Signal Effector. 2007;2505: 2493–2505. doi:10.1534/genetics.107.080994

75. Ho DM, Pallavi SK, Artavanis-tsakonas S. The Notch-mediated hyperplasia circuitry in Drosophila reveals a Src-JNK signaling axis. 2015; 1–21. doi:10.7554/eLife.05996

76. Roti G, Carlton A, Ross KN, Markstein M, Pajcini K, Su AH, et al. Complementary genomic screens identify SERCA as a therapeutic target in NOTCH1 mutated cancer. Cancer Cell. 2013;23: 390–405. doi:10.1016/j.ccr.2013.01.015

77. Krämer A, Mentrup T, Kleizen B, Rivera-Milla E, Reichenbach D, Enzensperger C, et al. Small molecules intercept Notch signaling and the early secretory pathway. Nat Chem Biol. 2013;9: 731–738. doi:10.1038/nchembio.1356

78. Shen CH, Chou CC, Lai TY, Hsu JE, Lin YS, Liu HY, et al. ZNRF1 Mediates Epidermal Growth Factor Receptor Ubiquitination to Control Receptor Lysosomal Trafficking and Degradation. Front Cell Dev Biol. 2021;9: 1103. doi:10.3389/FCELL.2021.642625/BIBTEX

79. Hoxhaj G, Caddye E, Najafov A, Houde VP, Johnson C, Dissanayake K, et al. The E3 ubiquitin ligase ZNRF2 is a substrate of mTORC1 and regulates its activation by amino acids. Elife. 2016;5: 1–18. doi:10.7554/eLife.12278

80. Sethna S, Scott PA, Giese APJ, Duncan T, Jian X, Riazuddin S, et al. CIB2 regulates mTORC1 signaling and is essential for autophagy and visual function. Nature Communications 2021 12:1. 2021;12: 1–19. doi:10.1038/s41467-021-24056-1

81. Sanz-Castillo B, Hurtado B, Vara-Ciruelos D, el Bakkali A, Hermida D, Salvador-Barbero B, et al. The MASTL/PP2A cell cycle kinase-phosphatase module restrains PI3K-Akt activity in an mTORC1-dependent manner. EMBO J. 2023;42. doi:10.15252/EMBJ.2022110833

82. Fatima I, Barman S, Uppada JP, Chauhan S, Rauth S, Rachagani S, et al. MASTL regulates EGFR signaling to impact pancreatic cancer progression. Oncogene. 2021;40: 5691–5704. doi:10.1038/S41388-021-01951-X

83. Montero-Melendez T, Nagano A, Chelala C, Filer A, Buckley CD, Perretti M. Therapeutic senescence via GPCR activation in synovial fibroblasts facilitates resolution of arthritis. Nature Communications 2020 11:1. 2020;11: 1–15. doi:10.1038/s41467-020-14421-x

84. Wang H, Huang F, Zhang Z, Wang P, Luo Y, Li H, et al. Feedback Activation of SGK3 and AKT Contributes to Rapamycin Resistance by Reactivating mTORC1/4EBP1 Axis via TSC2 in Breast Cancer. Int J Biol Sci. 2019;15: 929–941. doi:10.7150/IJBS.32489

85. Chivukula I v., Ramsköld D, Storvall H, Anderberg C, Jin S, Mamaeva V, et al. Decoding breast cancer tissue-stroma interactions using species-specific sequencing. Breast Cancer Research. 2015;17: 1–14. doi:10.1186/S13058-015-0616-X/FIGURES/4

86. Nicolas M, Wolfer A, Raj K, Kummer JA, Mill P, van Noort M, et al. Notch1 functions as a tumor suppressor in mouse skin. Nat Genet. 2003;33: 416–21. doi:10.1038/ng1099

87. Gosney JA, Wilkey DW, Merchant ML, Ceresa BP. Proteomics reveals novel protein associations with early endosomes in an epidermal growth factor- dependent manner. Journal of Biological Chemistry. 2018;293: 5895–5908. doi:10.1074/jbc.RA117.000632

88. Miura GI, Roignant J, Wassef M, Treisman JE. Myopic acts in the endocytic pathway to enhance signaling by the Drosophila EGF receptor. Development. 2008;135: 1913–1922. doi:10.1242/dev.017202

89. Ali N, Zhang L, Taylor S, Mironov A. Article Recruitment of UBPY and ESCRT Exchange Drive HD-PTP-Dependent Sorting of EGFR to the MVB. 2013; 453–461. doi:10.1016/j.cub.2013.02.033

90. Moberg KH, Schelble S, Burdick SK, Hariharan IK. Mutations in erupted, the Drosophila ortholog of mammalian tumor susceptibility gene 101, elicit non-cell-autonomous overgrowth. Dev Cell. 2005;9: 699–710. doi:10.1016/j.devcel.2005.09.018

91. Manteghi S, Gingras MC, Kharitidi D, Galarneau L, Marques M, Yan M, et al. Haploinsufficiency of the ESCRT Component HD-PTP Predisposes to Cancer. Cell Rep. 2016;15: 1893–1900. doi:10.1016/J.CELREP.2016.04.076

92. Lin G, Aranda V, Muthuswamy SK, Tonks NK. Identification of PTPN23 as a novel regulator of cell invasion in mammary epithelial cells from a loss-of-function screen of the 'PTP-ome''.' Genes Dev. 2011;25: 1412–1425. doi:10.1101/GAD.2018911

93. Gugger M, Reubi JC. Gastrin-Releasing Peptide Receptors in Non-Neoplastic and Neoplastic Human Breast. Am J Pathol. 1999;155: 2067–2076. doi:10.1016/S0002-9440(10)65525-3

94. Körner M, Waser B, Rehmann R, Reubi JC. Early over-expression of GRP receptors in prostatic carcinogenesis. Prostate. 2014;74: 217–224. doi:10.1002/PROS.22743

95. Kato A, Kondo N, Wanifuchi-Endo Y, Fujita T, Asano T, Hisada T, et al. Low TINAGL1 expression is a marker for poor prognosis in breast cancer. J Cancer Res Clin Oncol. 2022 [cited 23 Feb 2023]. doi:10.1007/S00432-022-04394-3

96. Shen M, Jiang YZ, Wei Y, Ell B, Sheng X, Esposito M, et al. Tinagl1 Suppresses Triple-Negative Breast Cancer Progression and Metastasis by Simultaneously Inhibiting Integrin/FAK and EGFR Signaling. Cancer Cell. 2019;35: 64-80.e7. doi:10.1016/J.CCELL.2018.11.016

97. Zhang H, Zhang LQ, Yang CC, Li J, Tian XY, Li DN, et al. The high expression of NUDT5 indicates poor prognosis of breast cancer by modulating AKT / Cyclin D signaling. PLoS One. 2021;16. doi:10.1371/JOURNAL.PONE.0245876

98. Wright RHG, Lioutas A, Dily F le, Soronellas D, Pohl A, Bonet J, et al. ADP-ribose-derived nuclear ATP synthesis by NUDIX5 is required for chromatin remodeling. Science. 2016;352: 1221–1225. doi:10.1126/SCIENCE.AAD9335

99. Sakurai T, Kamakura S, Hayase J, Kohda A, Nakamura M, Sumimoto H. GPR125 (ADGRA3) is an autocleavable adhesion GPCR that traffics with Dlg1 to the basolateral membrane and regulates epithelial apicobasal polarity. J Biol Chem. 2022;298. doi:10.1016/J.JBC.2022.102475

100. Spina E, Simundza J, Incassati A, Chandramouli A, Kugler MC, Lin Z, et al. Gpr125 is a unifying hallmark of multiple mammary progenitors coupled to tumor latency. Nature Communications 2022 13:1. 2022;13: 1–17. doi:10.1038/s41467-022-28937-x

101. Xu K, Usary J, Kousis PC, Prat A, Wang DY, Adams JR, et al. Lunatic fringe deficiency cooperates with the Met/Caveolin gene amplicon to induce basal-like breast cancer. Cancer Cell. 2012;21: 626–641. doi:10.1016/J.CCR.2012.03.041

102. Zhang S, Chung WC, Miele L, Xu K. Targeting Met and Notch in the Lfng-deficient, Met-amplified triple-negative breast cancer. Cancer Biol Ther. 2014;15: 633–642. doi:10.4161/CBT.28180

103. Huang KH, Sung IC, Fang WL, Chi CW, Yeh TS, Lee HC, et al. Correlation between HGF/c-Met and Notch1 signaling pathways in human gastric cancer cells. Oncol Rep. 2018;40: 294–302. doi:10.3892/OR.2018.6447

104. Gude NA, Emmanuel G, Wu W, Cottage CT, Fischer K, Quijada P, et al. Activation of Notch-mediated protective signaling in the myocardium. Circ Res. 2008;102: 1025–1035. doi:10.1161/CIRCRESAHA.107.164749

105. Stella MC, Trusolino L, Pennacchietti S, Comoglio PM. Negative feedback regulation of Met-dependent invasive growth by Notch. Mol Cell Biol. 2005;25: 3982–3996. doi:10.1128/MCB.25.10.3982-3996.2005

106. Yang YF, Wang YY, Hsiao M, Lo S, Chang YC, Jan YH, et al. IMPAD1 functions as mitochondrial electron transport inhibitor that prevents ROS production and promotes lung cancer metastasis through the AMPK-Notch1-HEY1 pathway. Cancer Lett. 2020;485: 27–37. doi:10.1016/J.CANLET.2020.04.025

107. Wu W, Sun XH. A mechanism underlying NOTCH-induced and ubiquitin-mediated JAK3 degradation. J Biol Chem. 2011;286: 41153–41162. doi:10.1074/JBC.M111.273755

108. Na J, Shin JY, Jeong H, Lee JY, Kim BJ, Kim WS, et al. JMJD3 and NF-κB-dependent activation of Notch1 gene is required for keratinocyte migration during skin wound healing. Sci Rep. 2017;7. doi:10.1038/S41598-017-06750-7

109. Cordier C, Prevarskaya N, Lehen'kyi V. TRPM7 Ion Channel: Oncogenic Roles and Therapeutic Potential in Breast Cancer. Cancers (Basel). 2021;13. doi:10.3390/CANCERS13246322

110. Liu M, Inoue K, Leng T, Guo S, Xiong Z gang. TRPM7 channels regulate glioma stem cell through STAT3 and Notch signaling pathways. Cell Signal. 2014;26: 2773. doi:10.1016/J.CELLSIG.2014.08.020

111. Wan J, Guo AA, King P, Guo S, Saafir T, Jiang Y, et al. TRPM7 Induces Tumorigenesis and Stemness Through Notch Activation in Glioma. Front Pharmacol. 2020;11: 1. doi:10.3389/FPHAR.2020.590723/FULL

112. Díaz-Tocados JM, Herencia C, Martínez-Moreno JM, Montes de Oca A, Rodríguez-Ortiz ME, Vergara N, et al. Magnesium Chloride promotes Osteogenesis through Notch signaling activation and expansion of Mesenchymal Stem Cells. Sci Rep. 2017;7. doi:10.1038/S41598-017-08379-Y

113. Yan D, Jin Y. Regulation of DLK-1 kinase activity by calcium-mediated dissociation from an inhibitory isoform. Neuron. 2012;76: 534–548. doi:10.1016/J.NEURON.2012.08.043

114. Tortosa E, Sengupta Ghosh A, Li Q, Wong WR, Hinkle T, Sandoval W, et al. Stress-induced vesicular assemblies of dual leucine zipper kinase are signaling hubs involved in kinase activation and neurodegeneration. EMBO J. 2022;41. doi:10.15252/EMBJ.2021110155

115. Ko SH, Apple EC, Liu Z, Chen L. Age-dependent autophagy induction after injury promotes axon regeneration by limiting NOTCH. Autophagy. 2020;16: 2052. doi:10.1080/15548627.2020.1713645

116. Mamaeva OA, Kim J, Feng G, McDonald JM. Calcium/calmodulin-dependent kinase II regulates notch-1 signaling in prostate cancer cells. J Cell Biochem. 2009;106: 25–32. doi:10.1002/JCB.21973

117. Choi YH, Ann EJ, Yoon JH, Mo JS, Kim MY, Park HS. Calcium/calmodulin-dependent protein kinase IV (CaMKIV) enhances osteoclast differentiation via the up-regulation of Notch1 protein stability. Biochim Biophys Acta. 2013;1833: 69–79. doi:10.1016/J.BBAMCR.2012.10.018

118. Qu J, Zhou Y, Li Y, Yu J, Wang W. CASK regulates Notch pathway and functions as a tumor promoter in pancreatic cancer. Arch Biochem Biophys. 2021;701. doi:10.1016/J.ABB.2021.108789

119. Chakravarti B, Yang J, Ahlers-Dannen KE, Luo Z, Flaherty HA, Meyerholz DK, et al. Essentiality of Regulator of G Protein Signaling 6 and Oxidized Ca2+/Calmodulin-

Dependent Protein Kinase II in Notch Signaling and Cardiovascular Development. J Am Heart Assoc. 2017;6. doi:10.1161/JAHA.117.007038

120. Mok K, Tsoi H, Man EP, Leung M, Chau KM, Wong L, et al. Repurposing hyperpolarization-activated cyclic nucleotide-gated channels as a novel therapy for breast cancer. Clin Transl Med. 2021;11: 11. doi:10.1002/CTM2.578

121. Giuli M v., Giuliani E, Screpanti I, Bellavia D, Checquolo S. Notch Signaling Activation as a Hallmark for Triple-Negative Breast Cancer Subtype. J Oncol. 2019;2019. doi:10.1155/2019/8707053

122. Endo A, Matsumoto M, Inada T, Yamamoto A, Nakayama KI, Kitamura N, et al. Nucleolar structure and function are regulated by the deubiquitylating enzyme USP36. J Cell Sci. 2009;122: 678–686. doi:10.1242/JCS.044461

123. Wang W, Lei Y, Zhang G, Li X, Yuan J, Li T, et al. USP39 stabilizes β-catenin by deubiquitination and suppressing E3 ligase TRIM26 pre-mRNA maturation to promote HCC progression. Cell Death Dis. 2023;14. doi:10.1038/S41419-023-05593-7

124. Havugimana PC, Hart GT, Nepusz T, Yang H, Turinsky AL, Li Z, et al. A Census of Human Soluble Protein Complexes. Cell. 2012;150: 1068. doi:10.1016/J.CELL.2012.08.011

125. Sun XX, He X, Yin L, Komada M, Sears RC, Dai MS. The nucleolar ubiquitin-specific protease USP36 deubiquitinates and stabilizes c-Myc. Proc Natl Acad Sci U S A. 2015;112: 3734–3739. doi:10.1073/PNAS.1411713112

126. Fraile JM, Campos-Iglesias D, Rodríguez F, Astudillo A, Vilarrasa-Blasi R, Verdaguer-Dot N, et al. Loss of the deubiquitinase USP36 destabilizes the RNA helicase DHX33 and causes preimplantation lethality in mice. J Biol Chem. 2018;293: 2183–2194. doi:10.1074/JBC.M117.788430

127. Taillebourg E, Gregoire I, Viargues P, Jacomin AC, Thevenon D, Faure M, et al. The deubiquitinating enzyme USP36 controls selective autophagy activation by ubiquitinated proteins. Autophagy. 2012;8: 767–779. doi:10.4161/AUTO.19381

128. Buszczak M, Paterno S, Spradling AC. Drosophila stem cells share a common requirement for the histone H2B ubiquitin protease scrawny. Science (1979). 2009;323: 248–251. doi:10.1126/SCIENCE.1165678/SUPPL_FILE/BUSZCZAK_SOM.PDF

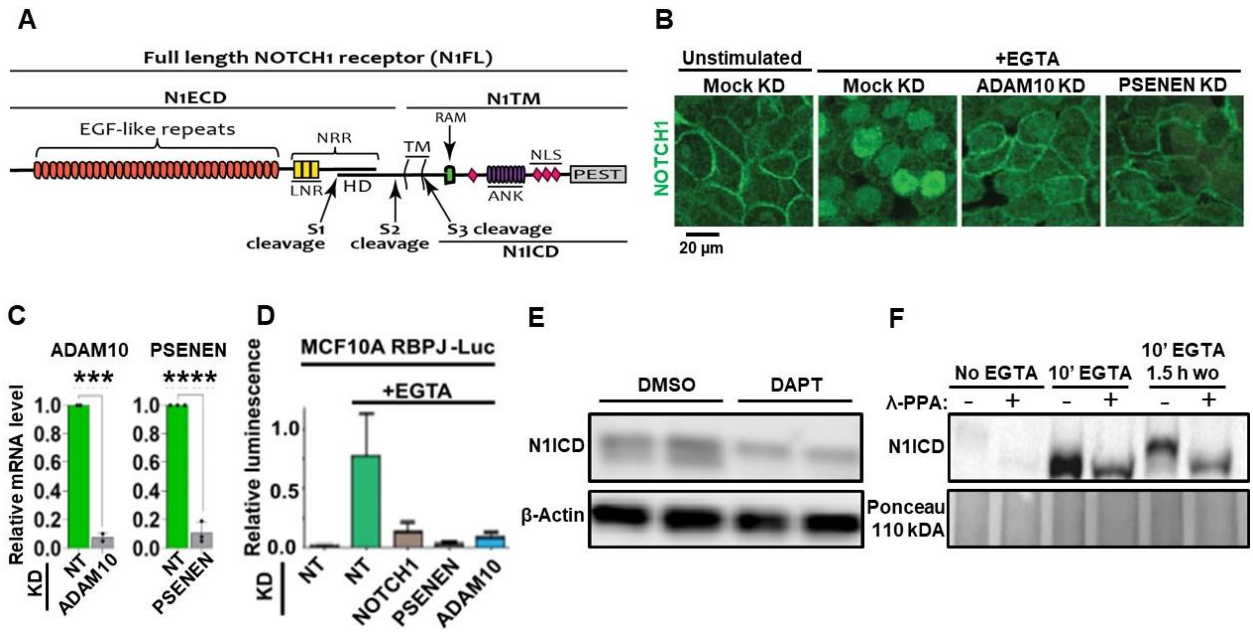

Fig. 1: Manipulation of endogenous NOTCH1 signaling in MCF10A cells. **(A)** The NOTCH1 (N1) full length receptor (N1FL) is composed of the N1 extracellular domain (N1ECD) and of the N1 transmembrane domain (N1TM). The N1ECD contains several EGF-like repeats, some of which are binding sites for Notch ligands as well as the negative regulatory region (NRR), which includes the Lin12/Notch Repeats (LNR) and the heterodimerization domain (HD). The N1ICD and N1ECD portions of Notch receptors are produced by Furin cleavage occurring at the S1 site during trafficking to the trans-Golgi network (TGN). N1ICD and N1ECD are non-covalently held together by Ca^{2+} at the HD. Ca^{2+} depletion causes ADAM10 and γ-secretase to sequentially cleave the receptor at S2 and S3 sites. This leads to the release in the cytoplasm of the N1 intracellular domain (N1ICD), which translocates to the nucleus. N1ICD contains the RBP-J-kappa-associated module (RAM), ankyrin repeats (ANK), nuclear localization signals (NLS), and the proline (P), glutamic acid (E), serine (S) and threonine (T) – PEST domain, which limits NICD half-life. **(B)** Immunofluorescence reveals that EGTA treatment relocates most endogenous N1 from the cell surface to the nucleus and this is inhibited by silencing *ADAM10* or *PSENEN*. **(C)** siRNA against *ADAM10* or *PSENEN* effectively deplete their mRNA. **(D)** The Notch reporter cell line, MCF10A-RbpJk-Luc, reports strong EGTA-induced Notch signaling, and this effect is markedly suppressed by silencing *NOTCH1, PSENEN* or *ADAM10*. **(E)** Western blot analysis of MCF10A cell extracts using an antibody against S3-cleaved N1 shows that unstimulated cells express low levels of N1ICD, which appears as a doublet. γ-secretase inhibition for 3 hours (DAPT) markedly reduces basal levels of the N1ICD lower band. **(F)** Western blot analysis of MCF10A lysates indicates that λ-phosphatase (λ-PPA) treatment leads to disappearance of the upper band of the N1ICD doublet, indicating that it corresponds to a phosphorylated N1CD form. *** and **** indicate $p < 0.001$ and $p < 0.0001$, respectively.

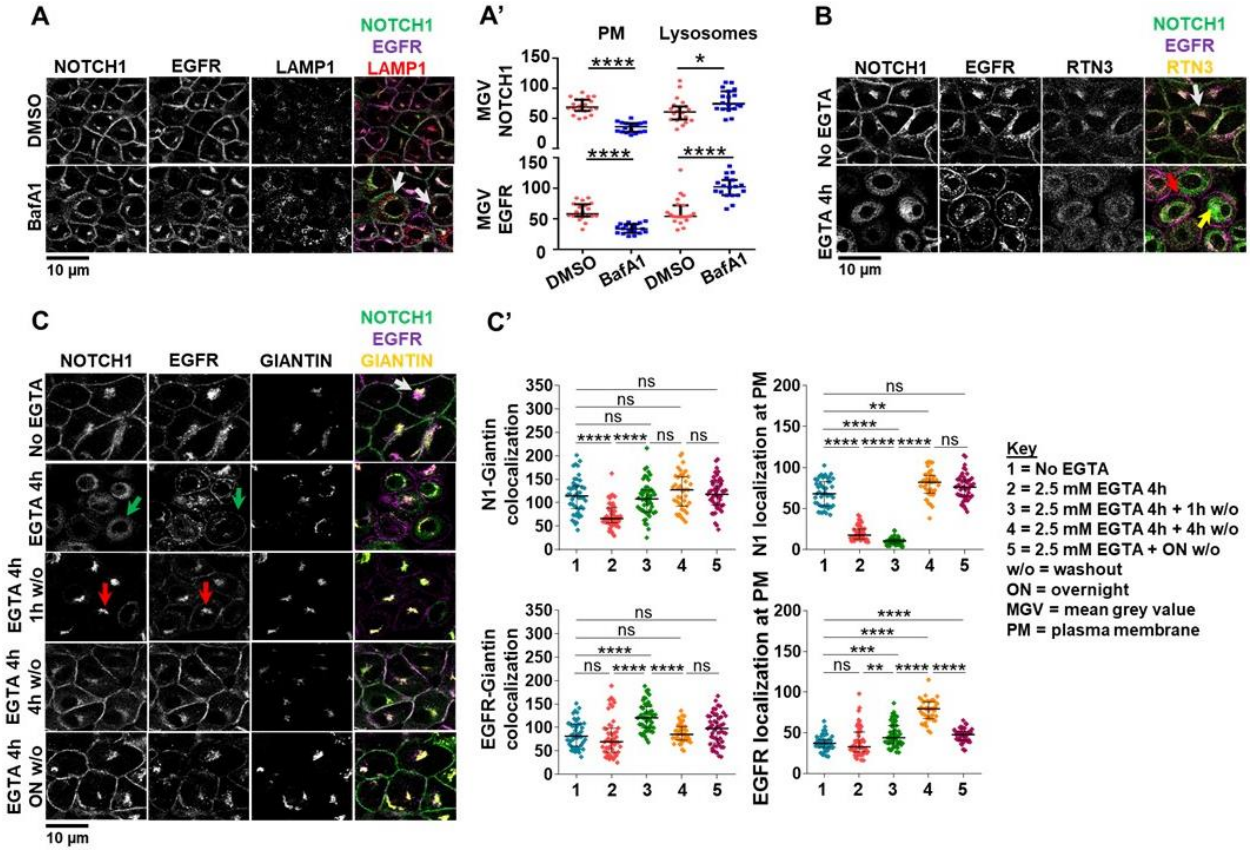

Fig. 2: Endocytic and exocytic endogenous NOTCH1 receptor trafficking in MCF10A cells. **(A)** Confocal sections of MCF10A cells treated and immunolabeled as indicated. Upon BafA1 treatment, plasma membrane (PM) localization of both NOTCH1 and EGFR is reduced and both receptors accumulate in LAMP1-positive compartments (arrowheads; quantified in A'). (**B**) Confocal sections of MCF10A cells treated and immunolabeled as indicated. 4-hour EGTA treatment depletes NOTCH1 from the PM and strongly accumulates it in a RTN3-positive compartment (yellow arrowhead), whereas EGFR remains on the PM (red arrowhead). In unstimulated cells, a pool of both NOTCH1 and EGFR is visible in the RTN3-positive compartment (white arrowhead). **(C)** Confocal sections of MCF10A cells treated and immunolabeled as indicated. An intracellular pool of NOTCH1 and EGFR colocalizes with the Golgi apparatus (GA) marker, GIANTIN (white arrowheads). Compared with non-EGTA treated cells, 4-hour EGTA treatment causes diffused NOTCH1 and EGFR accumulation in the cytosol, with some EGFR remaining on the PM (green arrowheads). The GIANTIN signal is also diffused consistent with an expected fragmentation of the GA. EGTA washout (w/o) for 1 hour causes all NOTCH1 and most EGFR signal to localize in the GA (red arrowheads). EGTA w/o for 4 hours or overnight (ON) restores normal intracellular distribution of NOTCH1 and EGFR (quantified in C'; *, **, ***, ****, ns indicate $p < 0.05$, $p < 0.01$, $p < 0.001$, $p < 0.0001$, and not significant, respectively).

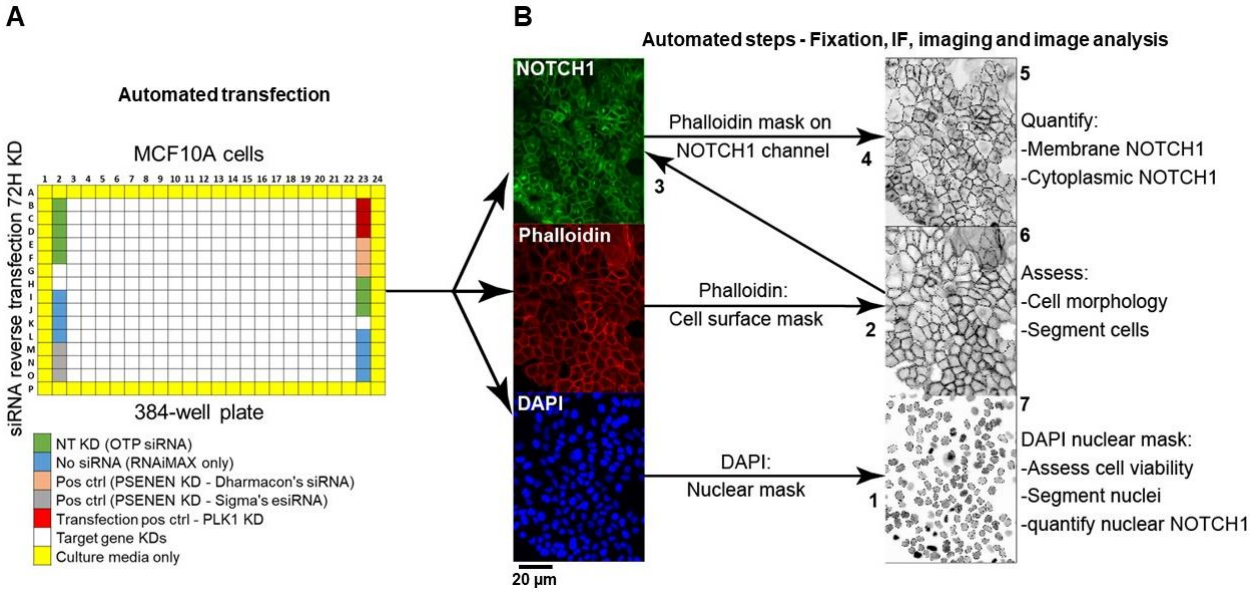

Fig. 3: High content screen pipeline and image analysis strategy. **(A)** The primary screen was performed on MCF10-A cells in a 384-well format. Genes belonging to a subset of the human genome, were knocked down in 6 replicate plates for 72 hours by RNAi along with the listed controls. In a duplicate experiment, cells were stimulated with EGTA. Control wells were distributed in the plates as shown. NT: non-targeting KD – cells were transfected with non-targeting siRNA. No siRNA: cells received RNAiMAX only. Pos ctrl (positive control) – cells were transfected with siRNA against *PSENEN*. Transfection pos ctrl: cells were transfected with siRNA against *PLK1* (Polo-like kinase 1) as a cytotoxic indicator of transfection efficiency. Outer wells (yellow) were filled with media to prevent evaporation in experimental wells. **(B)** To assess endogenous NOTCH1 localizations, cells in plates were subjected to automated IF and DAPI/Phalloidin labeling to demarcate nuclei and the cell cortex, respectively. The script steps of the image acquisition and analysis developed in-house are as follows: (1) The nuclei were segmented based on DAPI signal. (2) The cell surface was segmented using the phalloidin signal and overlaid on the NOTCH1 channel (3) to quantify levels of cell surface NOTCH1 (4) and the area between the cell cortex and the nuclei was used to determine levels of cytoplasmic NOTCH1 (5). (6) The phalloidin mask was also used to count cells and establish cell-to-cell boundaries. (7) Nuclear size was used a readout of cell viability as compact, pycnotic nuclei identify dead cells. Using such a pipeline, each gene KD was defined by its effects on the amount of NOTCH1 at the cell cortex, in the cytoplasm or in the nucleus.

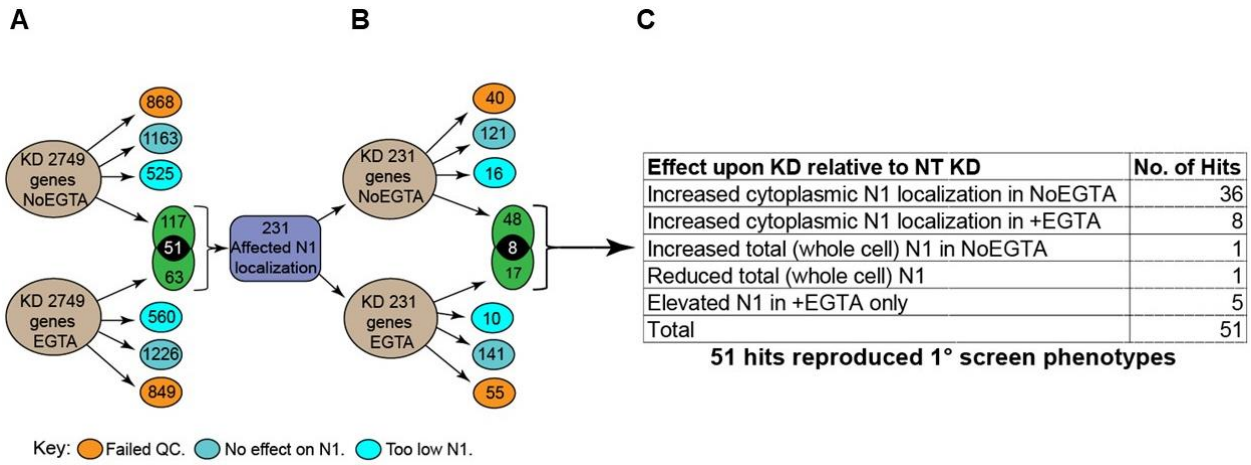

Effect upon KD relative to NT KD	No. of Hits
Increased cytoplasmic N1 localization in NoEGTA	36
Increased cytoplasmic N1 localization in +EGTA	8
Increased total (whole cell) N1 in NoEGTA	1
Reduced total (whole cell) N1	1
Elevated N1 in +EGTA only	5
Total	51

51 hits reproduced 1° screen phenotypes

Fig. 4: Schematics of the primary and secondary screens and of the candidate genes classification process. (A) A total of 2749 genes were silenced in the primary screen. Candidates that when compared with controls led to marked cytotoxicity or did not affect intracellular NOTCH1 (**N1**) localization, or caused general loss of NOTCH1 signal, were excluded from further analysis (orange, blue, and light blue circles, respectively). A total of 231 genes that altered intracellular NOTCH1 localization were identified (green). 117 did so in unstimulated condition, 63 upon EGTA stimulation and 51 in both conditions. **(B)** The 231 candidates underwent secondary screening. 73 of the 231 led to changes in NOTCH1 localization but only 51 genes reproduced the primary screen phenotypes. **(C)** Of these 51, 38 affected NOTCH1 trafficking in the unstimulated No EGTA condition, 8 altered NOTCH1 trafficking in the stimulated +EGTA condition.

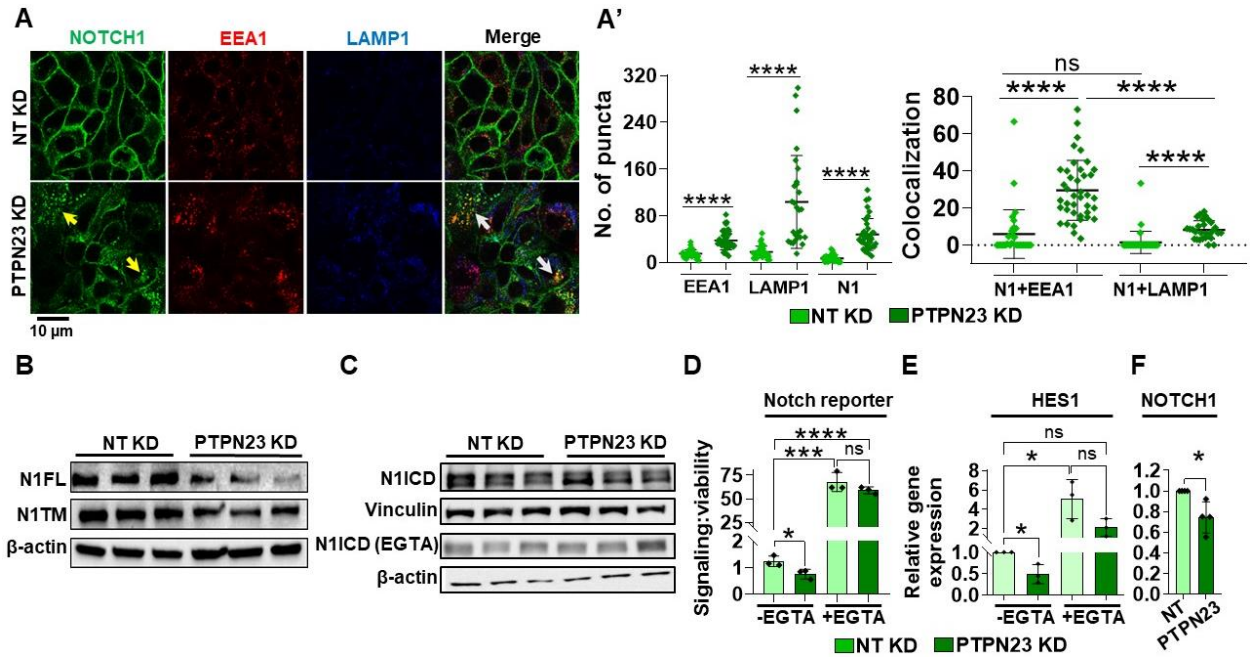

Fig. 5: Analysis of NOTCH1 localization and signaling activity upon *PTPN23* silencing. (A) Confocal sections of MCF10A cells treated and immunolabeled as indicated. *PTPN23* silencing causes marked increase in the number of EEA1, LAMP1 and NOTCH1 (N1) puncta, as well as accumulation of intracellular NOTCH1 positive puncta (yellow arrowheads), which mostly colocalize with EEA1 (white arrowheads; quantified in A'). **(B–C)** Western blot analyses indicate that *PTPN23* depletion reduces the levels of N1FL and N1TM but does not alter N1ICD levels with or without EGTA. **(F–H)** The Notch reporter cell line MCF10A-RbpJk-Luc and RT-qPCR analysis reveal that *PTPN23* depletion mildly suppresses basal Notch signaling. *, ***, ****, and ns indicates $p < 0.05$, $p < 0.001$, $p < 0.0001$, and not significant, respectively.

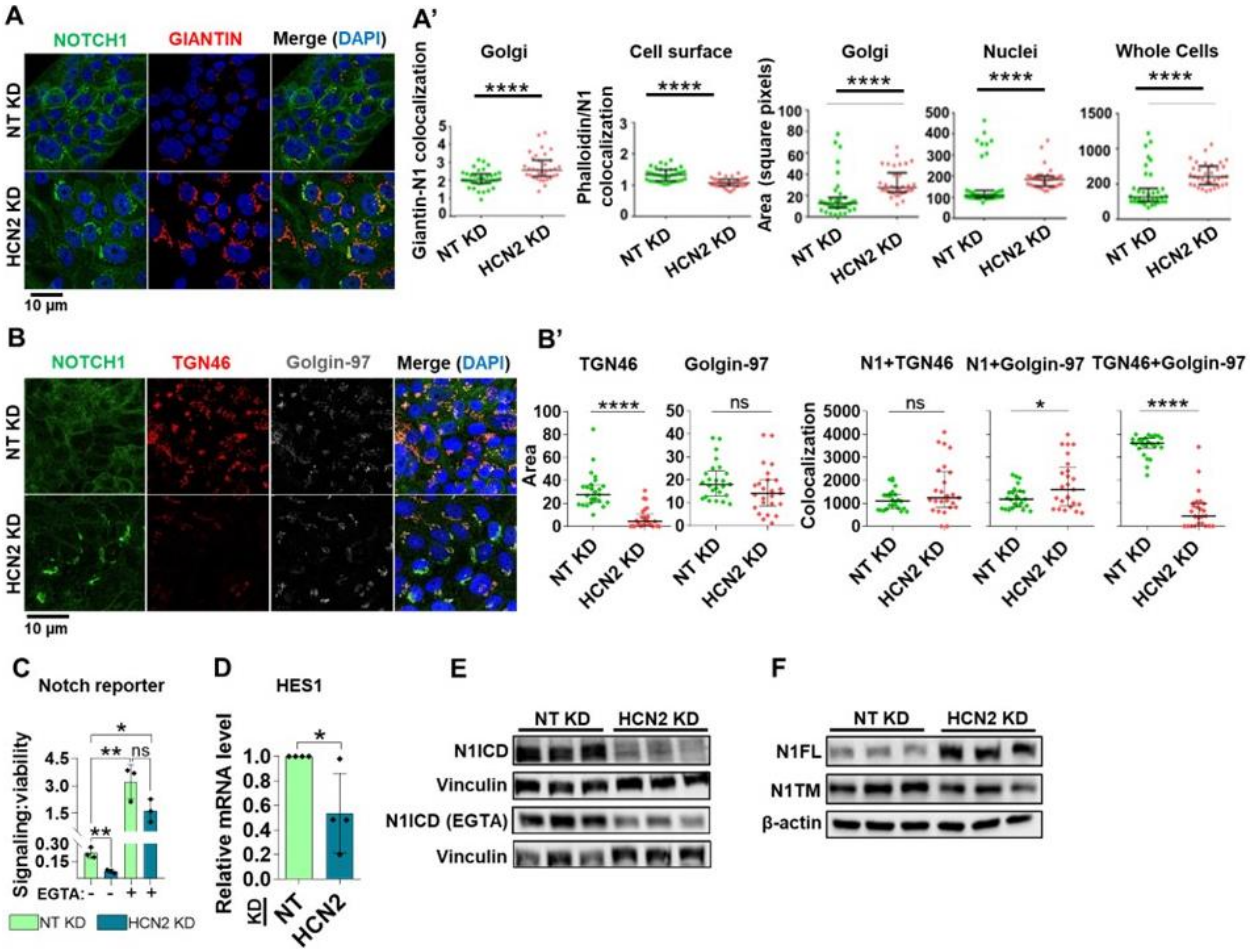

Fig. 6: Analysis of NOTCH1 localization and signaling activity upon *HCN2* silencing. (A) Confocal sections of MCF10A cells treated and immunolabeled as indicated. *HCN2* silencing causes marked NOTCH1 accumulation in the GIANTIN-positive compartment while significantly reducing cell surface NOTCH1 levels and enhancing cell size (quantified in A'). **(B)** Confocal sections of MCF10A cells treated and immunolabeled as indicated. *HCN2* silencing markedly depletes the TGN46-positive compartment but not the Golgin-97-positive compartment and causes NOTCH1 (N1) accumulation in the Golgin-97-positive compartment (quantified in B'). **(C–D)** The Notch reporter cell line, MCF10A-RbpJk-Luc and RT-qPCR analysis reveal that *HCN2* silencing suppresses basal Notch signaling. **(E)** Western blot analyses indicate that *HCN2* depletion reduces both basal and EGTA-stimulated N1ICD levels. **(E)** Western blot analysis indicates that *HCN2* silencing results in marked accumulation of N1FL. *, **, ****, and ns indicate $p < 0.05$, $p < 0.01$, $p < 0.0001$, and not significant, respectively.

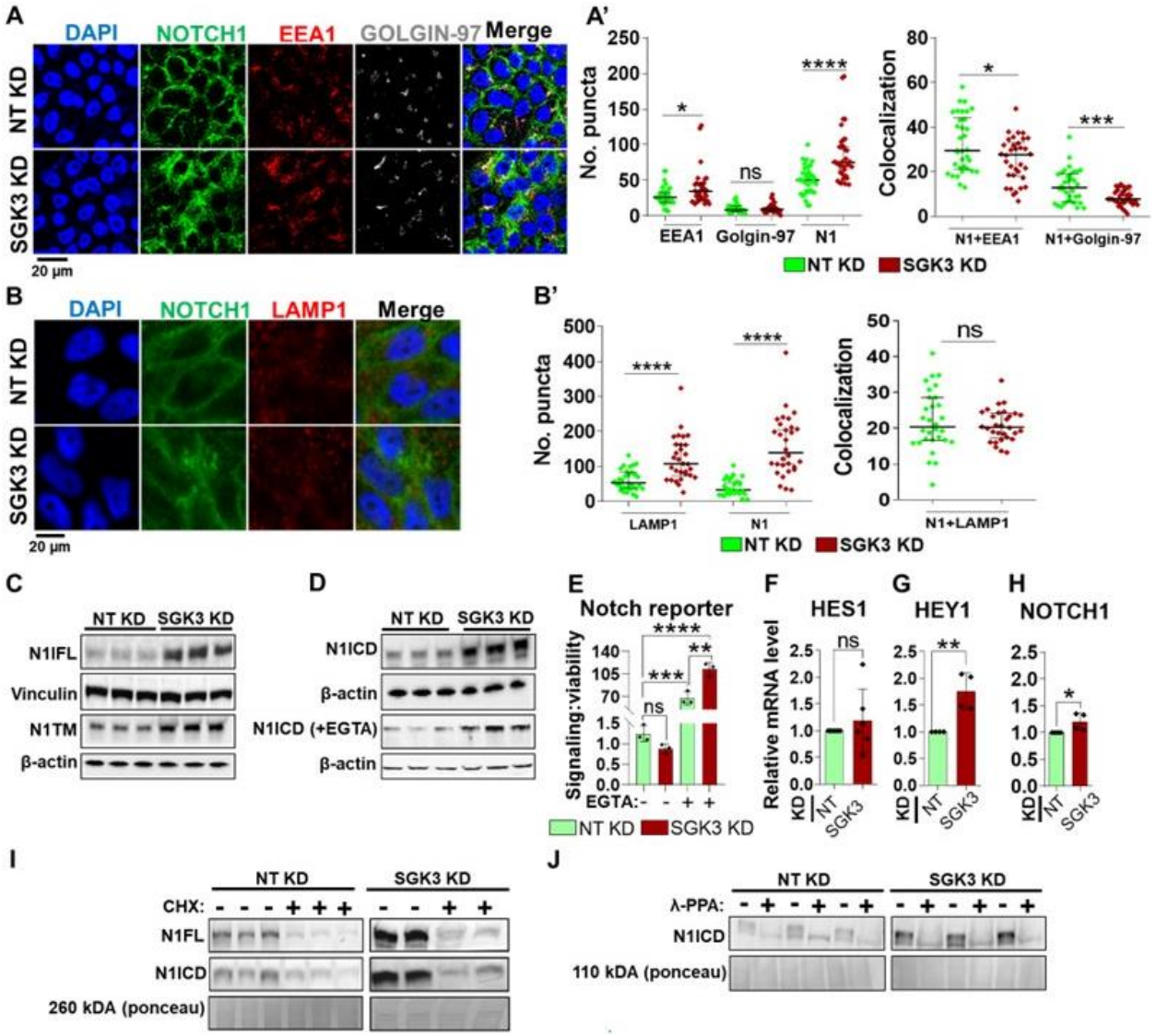

Fig. 7: Analysis of NOTCH1 localization and signaling activity upon *SGK3* silencing. (A) Confocal sections of MCF10A cells treated and immunolabeled as indicated. *SGK3* silencing causes NOTCH1 (N1) accumulation in the cytoplasm without apparent co-localization with EEA1 or GOLGIN-97 (quantified in A'). **(B)** Confocal sections of MCF10A cells treated and immunolabeled as indicated. The accumulated N1 upon *SGK3* silencing does not colocalize with LAMP1 (quantified in B'). **(C–D)** Western blot analyses show that *SGK3* depletion causes strong accumulation of all forms of the NOTCH1 receptor. **(E)** The Notch reporter cell line MCF10A-RbpJk-Luc reveals that *SGK3* silencing enhances Notch signaling in EGTA-stimulated cells. **(F–H)** RT-qPCR analysis of the Notch targets reveals that *SGK3* depletion enhances basal Notch signaling. **(I)** Western blot analyses indicate that SGK3 does not destabilize NOTCH1. **(J)** Western blot analyses of lysates treated with λ-phosphatase (λ-PPA) showed that similar to controls, most of the N1ICD that accumulates upon SGK3 silencing is phosphorylated. *, **, ***, ****, and ns indicate p <0.05, p <0.01, p <0.001, p <0.0001, and not significant, respectively.

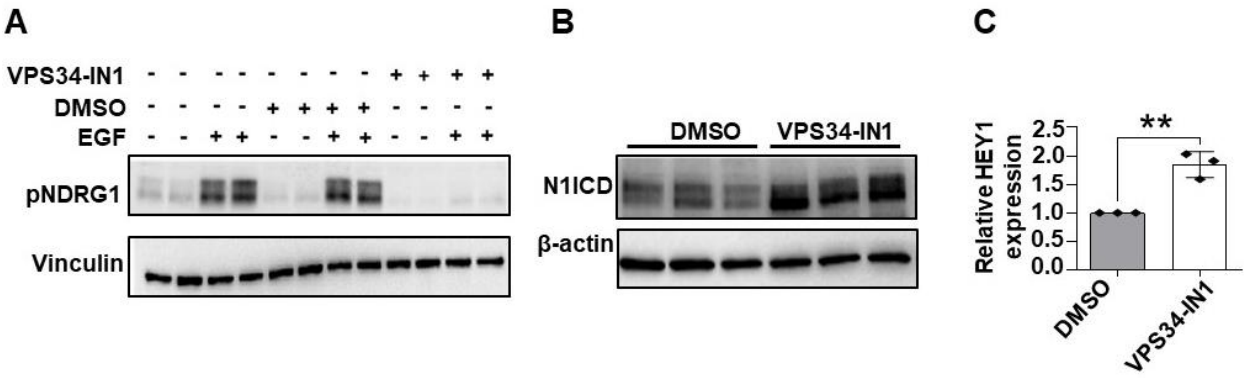

Fig. 8: Pharmacologic SGK3 inhibition elevates γ-secretase-derived N1ICD and Notch signaling. Western blot analysis reveals that serum-starved, VPS34-IN1-treated, MCF10A cells fail to phosphorylate NDRG1 (a SGK3 target) upon EGF stimulation. **(B)** Western blot analysis reveals that as with siRNA, pharmacologic VPS34-IN1 treatment enhances N1ICD levels. **(C)** RT-qPCR analysis shows that pharmacologic VPS34-IN1 treatment significantly enhances the expression of the Notch target gene HEY1. ** indicates p <0.01.

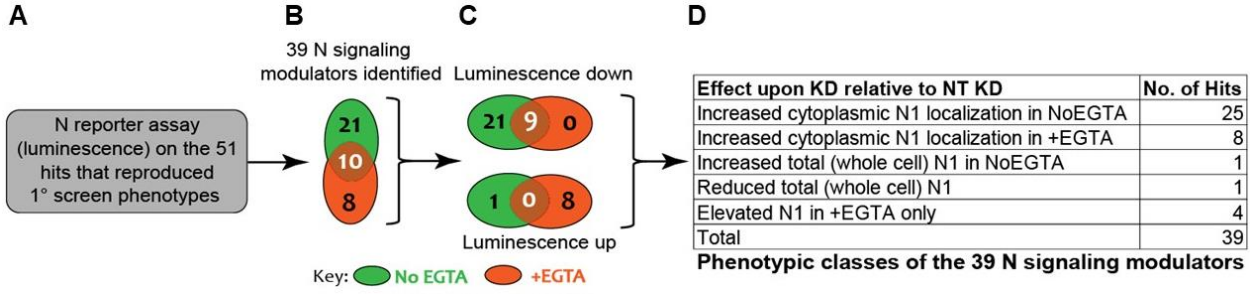

Effect upon KD relative to NT KD	No. of Hits
Increased cytoplasmic N1 localization in NoEGTA	25
Increased cytoplasmic N1 localization in +EGTA	8
Increased total (whole cell) N1 in NoEGTA	1
Reduced total (whole cell) N1	1
Elevated N1 in +EGTA only	4
Total	39

Phenotypic classes of the 39 N signaling modulators

Fig. 9: A secondary screen using a Notch reporter identifies 39 new signaling modulators. (A–B) MCF10A-RbpJk-Luc Notch reporter assay identifies 39 candidates that affect Notch signaling. **(C)** Of the 39, 30 suppress Notch signaling while 9 enhance Notch signaling. **(D)** Classification of the 39 candidates by their effect on intracellular NOTCH1 (N1) localization and/or levels.